Reliability analysis of lead-free solders for an aerospace application

Submitted by

Seyed Amir Mousavi Lajimi

Department of Mechanical Engineering
for the degree of Master of Science

Supervisors:
Dr. Joel Cugnoni
and
Professor John Botsis

Laboratory of Applied Mechanics and Reliability Analysis
Swiss Federal Institute of Technology Lausanne

January 2008

To those I love and those who wish me the best

Abstract

A deep analysis of the reliability of lead-free (SnAgCu) solders in comparison with tin-lead solders have been done for a particular aerospace application, SwissCube's motherboard (MB). Since 2006, using Pb in consumer electronics has been banned. Aerospace applications are not included in this legislation, however, sooner or later aerospace industry should comply with the general trend in the electronic industry because it is dependent on the whole industry for its components. Searching for a lead-free solder which presents high-reliability properties is still continued. SnAgCu solders have become popular in the electronics industry, because of the price and their mechanical properties. The creep properties of this solder composition, as the most important deformation mechanism under thermal loads, has been investigated in this thesis, and results have been validated with a thermal shock test. To simulate creep deformation in 2-dimension, one small electronic package, resistor, of SwissCube's motherboard was selected. Main constitutive relations have been implemented in a finite-element analysis software, to calculate creep strain evolution under thermal loads. The results of simulation suggest using, the new kind of solder, SnAgCu, would be even better for this type of package. For 3-dimensional analysis, one of the largest packages of the SwissCube's motherboard was simulated, using a conservative assumption in terms of constitutive relation from 2-dimensional analysis. The risk of failure for this package is not high, and it was not predicted to see a total failure after one thousand test cycle. Again, both solders show a good resistance to creep deformation, although SnAgCu shows a higher number of life cycles to failure from simulation results. Finally, a thermal shock test was performed to evaluate the reliability of solder joints practically. The test was performed for one thousand cycles. Temperature and output current were monitored. No cut in voltage was seen, while temperature followed a very close trend to thermal simulation result. Microstructural analysis has also been performed using metallography process and optical microscopy. Results of this investigation also shows that both solders are safe to be used up to one thousand cycles. Overall, both solders are highly reliable with this number of thermal cycles, however, SnAgCu shows higher life time under this type of loading.

Contents

List of Figures

List of Tables

Chapter 1

Introduction

1.1 Motivation

Lead containing solders have been used in the electronic industries for decades, and the long term reliability properties of these solders have been understood completely. Lead is an easily accessible material with very good soldering properties. However, its mammalian toxicity is the reason that it is being eliminated from applications where suitable substitutes have been found [1].
Tin-silver-copper (SnAgCu) alloy is recommended as the substitute of eutectic SnPb solder in the reflow soldering[1] by many international organizations. The transition for lead-free solder and lead-free process will bring many new reliability problems. Due to the higher melting temperature of SnAgCu solder, components and printed circuit boards (PCBs) must withstand a higher temperature under the lead-free reflow profile, and the surface finishes on PCBs must be compatible with the lead-free solder and process [3].
Engelmaier 2003 [4], already mentioned possible appearing problems with lead-free solder joint reliability: "Lead-free solders have creep rates up to 100 times slower than the creep rates of standard SnPb solders. The implication is that meaningful reliability tests cannot be very much accelerated; and that while the use of lead-free (LF) solder for consumer goods like cell phones is ok, it clearly can not as yet be recommended for high-reliability applications".
This is why it would be very interesting to asses the possibility of using LF-solders for an aerospace application, where the legislation still allows the implementation of conventional Sn-Pb solders. Although, investigating all the related reliability issues are impossible to achieve in the defined objectives of this project, especially considering the time constraints.

1.2 Approaches

There are two common ways to approach the reliability issues, either doing some reliability tests or/and finite element analysis (FEA). FEA especially becomes

[1] Reflow soldering is the most common means to attach a surface mounted component to a circuit board, and typically consists of applying solder paste, positioning the devices, and reflowing the solder in a conveyorized oven [2].

very important when this is not possible to accomplish a complete reliability test due to the lack of some resources or time.

1.2.1 Reliability test

For the reliability assessments of solders different methods have been proposed in the literature, however the most common reliability tests includes thermal cycling test, thermal shock test, and vibration test. For the objective of this project, and considering the availability of the test device, thermal shock test was chosen and the designed boards were tested for a period of two weeks.

1.2.2 Finite element analysis

The ability of finite element method in predicting thermal strains/stresses, and induced inelastic strains in the materials, makes it a unique powerful device in most of the cases where there is no exact analytical solution for a problem.

1.3 Contributions

The main goal of this project is to follow a suitable methodology to assess the reliability of lead-free (SnAgCu) solders for a special case, where in the corresponding application solder is mainly under thermal loads. The objectives of this project are listed below:

- Literature review on the solder reliability.
- Simulating and predicting the temperature variation with time and location on the SwissCube's[1] motherboard.
- Simulating creep behavior of the solder joints for one package in 2-dimension.
- Simulating creep behavior of the solder joints for one package in 3-dimension.
- Correlate the results of creep simulation with the number of life cycles to failure.
- Validate results of the simulation with a thermal shock test.
- Microstructural analysis of solder joints after thermal shock test.
- Make a conclusion based on FEA and experimental analysis.

1.4 Report organization

Chapter 2 contains a literature review on the reliability analysis of lead-free solders with a brief explanation about the main mechanical phenomenon. In Chapter 3 the implementation of finite element method and the realization of the test are explained. The results of those implementations are presented in Chapter 4, with a discussion about the results of this work. The conclusions and future works are given in Chapter 5.

[1] SwissCube is a small satellite, to be launched end-2008. This satellite follows the CubeSat standard (1kg cube with a 1 liter volume) providing a fast and affordable access to space.

Chapter 2

Reliability analysis of solder joints

2.1 Overview

According to the European Union Waste Electrical and Electronic Equipment Directive (WEEE) and Restriction of Hazardous Substances Directive (RoHS), lead had to be eliminated from consumer electronic systems by July 1^{st} 2006, leading to much interest in lead-free solders, while there is still no legislation regarding high reliability applications such as military or aerospace applications. During these years SnAgCu (SAC) solder alloys have attracted too much attention as the best possible replacement of the tin-lead conventional solders. As a result, studying the long-term reliability of SnAgCu solders has gained too much attention from researchers in the field of reliability and mechanics of materials. This chapter would give a rather complete review of the achievements in the field of reliability of solders, mainly SnAgCu solders and SnPb in some cases, for the two different approaches; finite element method and experimental method. In some cases, the reliability tests have been done along with finite element analysis, and finally some microstructural analysis have been performed.
In the following sections, the role of solder in the electronic industry, reliability of solder joints, role of creep deformation in the solder joints, finite element analysis (FEA) and requirements, constitutive relations, life prediction methodology, experimental procedures and microstructural analysis, and finally, main results of the investigations by other researchers are discussed in details.

2.2 Soldering and Solder

Soldering is the most practical joining method that uses low-melting-point alloys, the solder, to join the electrical packages to the substrate. In the huge electronic applications, solder is an irreplaceable material in the assembly process; as a joining material, solder provides electrical, thermal and mechanical continuity in electronic assemblies. As it is clear, the quality of soldering and the solder are two crucial elements of the integrity of a solder joint, which is vital to the overall functioning of the assembly by itself. Forming mechanical bonds, the shrinking interconnects' size brings solder joint reliability to the forefront.

Considering different operating conditions, the solder joints could experience various kinds of loadings; this includes overstress, thermal cycling, vibration and shock, and cyclic bending of cuicuit boards. As a result of every loading condition the solder may plastify, creep or rupture, while the first two are considered as the pricipal deformation mechanisms in the solder joint. The effect of each one is determined according to the operating condition, for example where the solder does not experinece too much stress the role of creep is more important than plasticity. This especially happens when the package goes through a thermal cycle not a mechanical cycle like bending or shock, and the operating temperature is around or bigger than half of the melting temperature in absolute scale.

2.3 Reliability of solder joints

For a long time SnPb has been the most reliable solder alloy used in the most conventional electronic devices. As a natural result of this harmony, the most important mechanical properties of this solder that influences the reliability of solder joints are known. Since 2006, governments, organizations, and companies in several countries recommend or require the use of non-toxic solders in electronic or electrical products. The European union directives on WEEE and the RoHS stipulated that electronic equipment sold to European consumers be lead-free as of July 1^{st} 2006, while there is still no legislation or directives to limit using leaded solders in aerospace products or some other high reliability applications.
Nonetheless, since aerospace industry depends on the larger electronics industry for electronic materials, components, and assemblies, aerospace industry will be in a position that it should comply with environmental legislation which is restricting the use of toxic materials such as lead(Pb). One of the greatest concerns in using lead-free solders is the lack of long term reliability data.
Many different solder compositions have been proposed as a substitute for SnPb solders, for example SnAg, SnAgBi, SnAgCu, SnZn, SnCuIn, and SnAgBiCuGe [5]. Common to all these new lead-free solders is that tin (Sn) remains their basic element in most of them. The industry has shown a lot of interest in SnAgCu-based solders, and it seems that this solder composition may well become the most popular solder in the near future. The reasons for this are the competitive price, its mechanical properties, and a comparatively low melting point. However, variations in the amount of silver and copper can significantly affect the reliability and the mechanical properties of that alloy since the concentration of those elements in a solder matrix is relatively very small. In the case of SnPb solder, variations in the concentration of Pb were not so critical because of the high amount of Pb in the solder matrix.
Thermal fatigue is a primary threat to the reliability of solder joints. Soldered joints are thermally cycled in service, and are stressed in each thermal cycle due to inhomogeneities in the pattern of heating and the mismatch of coefficient of thermal expansion (CTE). The dominant stresses tend to be in shear, as a result of CTE mismatch between solder and package or substrate. Since the operating temperatures of microelectronic devices are a significant fraction of the melting temperatures of the solders used, the solders deform in high-temperature creep,

and joints eventually fail by creep fatigue or as it is called "Low Cycle Fatigue" (LCF). Summarizing, understanding of creep behavior and creep mechanisms is fundamental to the design of reliable joints [6].

2.4 Creep and creep behavior of solder joints

Creep is the term used to describe the tendency of a material to move or to deform permanently to relieve stresses. Material deformation occurs as a result of long term exposure to levels of stress that are below the yield strength or ultimate strength of the material. Creep is more severe in materials that are subjected to heat for long periods and near melting point. Creep is a monotonically increasing function of temperature [7].
Under constant load or stress, solder undergoes progressive inelastic deformations over time. This time-dependent deformation is called creep and the associated strains that develop over time are creep strains. When the test specimen is subjected to a constant load, the initial, instantaneous response includes elastic and time-independent plastic flow. Creep then proceeds in three stages of primary, secondary and tertiary creep, see Fig. 2.1.

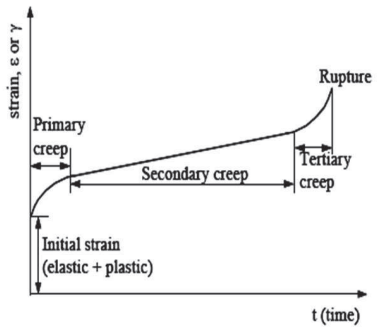

Figure 2.1: Creep curve: strain versus time under constant stress (or load) and temperature.

During primary creep, metals strain-harden. The strain rate decreases over time, as hardening of the metal becomes more difficult. Specimen deformations keep increasing with secondary creep proceeding at a steady strain rate. Note also that the initial deformation that occurs upon loading of the test specimen includes both elastic and plastic strains. Often, these initial deformations are not reported on in the context of creep studies. However, they can not be neglected, a priori, because of the inelastic nature of the initial plastic flow. Moreover, these initial deformations, which depend on the loading rate, may become important under service conditions with intermediate to rapid temperature ramps [8].
The temperature range in which creep deformation may occur differs in various materials. Generally, the minimum temperature required for creep deformation to occur is 30-40% of the melting point for metals and 40-50% of melting point for ceramics. Virtually any material will creep upon approaching its melting

temperature. Since the minimum temperature to see creep, is relative to melting point, creep can be seen at relatively low temperatures for some materials. [7].
As mentioned before, the ratio of operating and melting temperature in absolute scale, the "homologous temperature", demonstrates the importance of creep among other deformation mechanisms. The melting point of the most conventional solder alloy, Sn37Pb (eutectic), is 183 °C and for SnAgCu (Ag: 3.0 - 4.0%, Cu: 0.5 to 1.0%) the melting temperature is typically observed as 217 °C. This means that the homologous temperature (the ratio of operating and melting temperature in absolute scale) is about 0.51 for Sn37Pb and 0.47 for SnAgCu at -40 °C. It is well documented that creep plays a very important role in deformation behavior of materials at homologous temperatures close to and above 0.5 if the loading rate is slow enough for creep deformations to occur. Since in actual use conditions, the temperature cycle duration is in the order of minutes to days and the homologous temperature is more than 0.5, solder joints formed by using SnAgCu (or SnPb) solder alloys are expected to deform primarily due to creep [8].

2.5 Modeling of creep

As previously mentioned, solder interconnects are used to provide:

- Electrical connection between package and the substrate.
- Mechanical binding between package and substrate.
- Heat diffusion from the package.

Because the coefficients of thermal expansion (CTE) are different between the package, ceramic or polymer, and substrate (ceramic or polymer), tensile and/or shear strains occur in the solder interconnects when the device is powered on and heat is generated. If the device is powered on and off, or the temperature of the environment fluctuates periodically, such heat induced tensile/shear strain within interconnects is as a result cyclic - causing thermo-mechanical fatigue failure. It is thus essential to simulate the performance of any new material in order to assess its reliability before using it widely.
However, as mentioned before, when the solder is operating above half of its melting point and the magnitude of the induced thermo-mechanical stress/strain is not so big, creep processes are expected to dominate the deformation kinetics. For nonlinear numerical simulation of creep strain accumulation, a constitutive model of the material must be used which relates the stress and temperature to the strain rate. Finally, the induced accumulated creep during each cycle is obtained by integrating the constitutive relation during each cycle.
Since creep properties, as well as strength and other mechanical properties, vary with specimen size, the mechanical response of tiny solder joints differs from that of bulk solder test specimens. For engineering applications dealing with surface-mount (SM) assemblies, constitutive models developed from measurements on solder joint specimens have proven to be very useful. Solder deformations, including creep, have been measured on solder joints of actual

electronic assemblies and for several solder alloys. These models are presented, briefly, hereafter because they have been found to be useful in modeling creep deformation.
The creep deformation behavior of eutectic Sn/Pb solder alloy has been extensively studied and it has generally been observed that the steady state response depends on the applied stress. At least two different mechanisms have been identified; one operating at low stresses and high temperatures (grain boundary sliding or dislocation glide) and the other at high stresses and low temperatures (dislocation climb). Mathematically, the steady state creep strain rate is represented by either a *Dorn* type equation,

$$\dot{\epsilon} = A\sigma^n \exp \frac{-Q}{RT} \tag{2.1}$$

where A is a material constant, Q is an apparent activation energy, and R is the universal gas constant, or by sinh equation which generally looks like this:

$$\dot{\epsilon} = A\left[\sinh\left(\alpha\sigma\right)\right]^n e^{-\frac{Q}{RT}} \tag{2.2}$$

where again A is a material's constant, σ is stress, n is the constant exponent, and R is the universal gas constant, and both have been used to describe the creep deformation behavior of eutectic Sn/Pb solder in the literature [9].
There are also a number of published papers on the constitutive equation for creep deformation for SnAgCu alloy for compositions currently in considerations. Mathematically, the steady-state creep strain rate is represented by either Eq. 2.1 or Eq. 2.2. In the following, a number of pulished constitutive models for tin-lead and SnAgCu are disscussed.

2.5.1 Darveaux's constitutive relation

Darveaux and *Banerji* 1992 [10], and *Darveaux et al.* 1995 [11], have done a significant amount of tests on actual soldered assemblies to properly account for the effects of grain and intermetallic compound distribution. Tensile and shear loading were employed in the strain rate range between 10^{-8} to 10^{-1} s^{-1} and the temperature rang between 25 °C and 130 °C.
They suggested to use a sinh law, according to *Frost* and *Ashby* 1982 [12]; at intermidiate stresses, the strain rate depends on stress to power, n. At high stresses, the strain rate is an exponential function of stress. This power law breakdown region can be described by a single expression [12]:

$$\dot{\epsilon} = C_1 \frac{G}{T}\left[\sinh\left(\alpha\frac{\sigma}{G}\right)\right]^n e^{-Q/RT} \tag{2.3}$$

where C_1 is a constant, G is the temperature dependent shear modulus, T is temperature in absolute scale, R is the universal gas constant, α prescribes the stress level at which the power law dependence breaks down, and Q is the activation energy.
To obtain the true activation energy, the temperature dependence of the shear modulus must be incorporated

$$G = G_1 - G_0 T^{'}(^{\circ}C) \tag{2.4}$$

Table 2.1: Creep model constants by *Darveaux* [10].

	Solder Alloy Deformation Constant					
	Elastic		Steady state creep			
Solder	G_0	G_1	C_1	α	n	Q
	$10^6 lbf/in^2$	$10^3 lbf/in^2$	$k/s/lbf/in^2$			ev
60Sn40Pb						
Shear	1.9	8.1	0.198	1300.0	3.3	0.548
Tensile	5.0	22.0	0.114	751.0	3.3	0.548

$1\ ev = 96489\ Jmol^{-1}$

where G_0 is the shear modulus at 0 °C, G_1 gives the temperature dependence, and $T^{'}$ is the temperature in °C. The required constants by *Darveux* are presented in Table 2.1.

To derive inelastic tensile constants from shear constants authors used the following relations assuming that Von Mises yield criteria apply [13]:

$$\sigma = \tau\sqrt{3} \tag{2.5}$$

and

$$\epsilon = \frac{1}{\sqrt{3}}\gamma \tag{2.6}$$

2.5.2 Pao's constitutive relation

Pao et al. 1994 [14], performed thermal cyclic shear stress/strain test and determined hysteresis response of 63Sn-37Pb solder joints using a double beam specimen. The temperature cycle had a period of 40 minutes and extreme temperatures of 40 °C and 140 °C. The steady state creep properties of these solders were determined, and associated *Norton's* law was implemented in a finite element program to simulate the experiment. The fatigue life of these solders joints and failure mechanism were also discussed by these authors. The corresponding steady-state creep properties and associated mechanisms for Sn-37Pb eutectic are as follows: *Norton's* law:

$$\dot{\gamma} = B \cdot \tau^n \exp(-\frac{\Delta H}{KT}) \tag{2.7}$$

and the required constants are given in Table 2.2.

Table 2.2: Creep model constants by *Pao* [14].

Alloy	Deformation Mechanisms	B $MPa^{-n}.s^{-1}$	ΔH eV	n 40°C	n 140°C
Sn37Pb	dislocation glid/climb	0.205	0.49	5.25	5.25

2.5.3 Osterman's constitutive relation

Osterman and *Dasgupta* 2007 [15], report the required constants for *Garofalo's* model which is actually a sinh, see Eq. 2.2, because the data indicates a clear transition of the creep mechanism within the stress ranges of interest. This transition is manifested as a change in the slope of the creep-rate versus stress curves (on a loglog scale). The creep parameters are presented in Table 2.3. Based on

Table 2.3: Creep model constants by *Osterman* [15].

Solder alloy	A	α	n	Q.
Sn37Pb	1.15E4	0.20	2.2	5.93E4
Sn3.9Ag0.6Cu	1.50E3	0.19	4.0	7.13E4

physical measurements they found out that, the Pb-free SAC solder has been found to be significantly more creep resistant than Sn37Pb at low stress levels, (1 MPa), where the creep mechanisms are predominantly diffusion- driven. However, at higher stress levels, (10 MPa), creep mechanisms are predominantly dislocation- driven, and both solders have comparable creep. This finding, in part, explains the longer life observed for the Pb-free SAC solder, in direct comparisons of temperature cycling test results between SAC and Sn37Pb, in their case. This result also explains, in part, why acceleration factors for accelerated thermal cycling are higher for SAC solders than for SnPb solder.

2.5.4 Zhang's constitutive relation relation

Zhang et al. 2003 [16], used a one-dimensional incremental model of the test setup to simulate constant-load creep. They performed monotonic, and isothermal cyclic mechanical tests over various temperatures, strain rates and stresses using a thermo-mechanical-microstructural (TMM) test system. By fitting simulation results to constant-load creep and monotonic testing data, the primary creep, secondary creep and plastic models were achieved for both Sn3.9Ag0.6Cu and Sn37Pb solders.
They report the steady-state shear creep strain rate by using a sinh law, see Eq. 2.2, and the model constants for both solders are presnted in Table 2.4.

Table 2.4: Creep model parameters by *Zhang* [16].

Solder Alloy	A	α	n	Q
Sn37Pb	1999.4	0.2	2.1083	54137.2
Sn3.9Ag0.6Cu	248.4	0.188	3.7884	62916.7

2.5.5 Schubert's constitutive relation

Constants of different lead-free solder alloys have been determined by *Schubert et al.* 2003 [17], see Table 2.5, using 108 data points from their measurement and literature.

Table 2.5: Creep model parameters by *Schubert* [17].

Solder Alloy	A (s^{-1})	α MPa^{-1}	n	Q ev
Sn95.5Ag3.8Cu0.7 Sn95.75Ag3.5Cu0.75 Sn96.5Ag3.5Cu0.5	277984	0.02447	6.41	0.56

2.5.6 Kariya's constitutive relation

The *Kariya* model is a power-law model that did fit the *Kariya et al.*'s 2001 [18], Sn-3.0Ag-0.5Cu and Sn-3.8Ag-0.7Cu data equally well. The Kariya model gives steady state strain rates as a function of stress and absolute temperature T :

$$\dot{\epsilon} = A \left[\frac{\sigma}{E}\right]^n \exp \frac{-Q}{KT} \tag{2.8}$$

where $A = 1.37 \times 10^{46}$, $n = 13.2$, and $Q = 61000\ J/mole$ with: $E(MPa) = 76087 - 109 \times T$. The *Kariya* model fits the *Kariya* and *Neu et al.* 2001 [19], datasets nicely except for a slight departure from the data at -55 °C and strain rates above $10^{-3}/sec$. The Kariya model does not fit *Schubert*'s data [8].

NIST

A review on the available SAC data was done by National Institute of Standards and Technology [20]in 2004 considering datasheets by *Schubert et al.* [17], *Kariya et al.* [18] and *Neu et al.* [19]
A power-law breakdown creep model was considered and by regression analysis the coefficients of such a law were determined. The corresponding data covers:

- Temperatures in the range -55 °C to 150 °C.
- Stresses in the range 2 MPa to 100 MPa.
- Strain rates in the range 3.8×10^{-9}/sec to 1×10^{-3} /sec.

The corresponding constants of the sinh is presented in the following table, Table 2.6.

Table 2.6: Creep model parameters by *NIST* [20].

Solder Alloy	A (s^{-1})	α MPa^{-1}	n	Q $J/mole$
SAC	7.925×10^5	0.0356	6	67900

2.5.7 Pang's constitutive relation

Pang et al. 2005 [21], performed constant load creep tests at three different temperatures (25 °C, 75 °C, and 125 °C) with constant load set for several different stress levels (2, 3, 5, 7, 10, 15, 20, 25, 30, 35, and 40 MPa). They measured steady-state creep strain rate is plotted versus stress. Finally, a curve

fitted to the steady-state creep strain rate using a hyperbolic-sine, Eq. 2.2. The author's constants of creep model for 95.5Sn-3.8Ag-0.7Cu alloy is presented in Table 2.7.

Table 2.7: Creep model parameters by *Pang* [21].

Solder Alloy	A (s^{-1})	α MPa^{-1}	n	Q ev
Sn95.5Ag3.8Cu0.7	501.3	0.0316	4.96	0.47

2.5.8 Lau's constitutive relation

Lau et al. 2003 [22], used the same equation as *Pang et al.*'s, and accourding to their work the constants are as follows: $A = 4.41 \times 10^5$, $n = 4.2$, and $Q = 45000\ J/mole$.

2.5.9 Wiese's constitutive relation

In 2003, *Wiese et al.* [23], presented constitutive models for eutectic SnAgCu solders. Experimental investigations were carried out on specimens of different microstructures. The three specimen types have been flip-chip solder joints, pin through hole solder joints and standard bulk solder specimens. Constant-load creep tests were carried out on all three specimen types at temperatures between 5 °C and 70 °C. Creep data was taken for strain rates between 10^{-10} and 10^{-3}. Strain-stress-curves were recorded from the "flip-chip solder joint" specimens, using a micro shear tester. The microstructural properties of the bulk specimens and real solder joints were examined using metallographic sectioning, optical microscopy techniques, and SEM microprobe analysis. The results of the microstructural analysis were related to the investigated mechanical properties of the solders. The proposed creep model for SnAg4Cu0.5 is a power law equation that could be implemented using finite element analysis softwares, see Eq. 2.9.

$$\dot{\epsilon} = A(\sigma)^n \exp \frac{-Q}{KT} \tag{2.9}$$

where $A = 2 \times 10^{-21}$, $n = 18$, and $Q = 83.1 KJ/mole$, with T in K, σ in MPa.

2.6 Life prediction methodology

A number of life prediction models have been proposed in the literature for SnPb solder and more recently for SnAgCu solder interconnects. These models are either based on strain range, accumulated creep strain, or accumulated creep strain energy density during a temperature cycle. The basic assumption for most of these life prediction models is that the damage in solder joint during temperature cycling is primarily due to steady state creep strain accumulation. Although the primary creep and time independent plasticity may play a role, it is assumed that these effects are minor and can be included in a strain rate model as has been done by *Darveaux et al.* 1992 and 1995, or by other researchers, as previously mentioned. A number of these prediction laws are presented here.

2.6.1 Syed's approach and models

Syed 2001 [9] and 2004 [24], used a step by step approach to establish a life prediction law for SnAgCu solder joints by using "sinh" type constitutive relation[1].
The "Monkmann-Grant" equation for creep rupture, as given in Eq. 2.10, states that the time to rupture, t_r, is inversely related to the steady state creep strain rate, $\dot{\epsilon}_{cr}$, during a test.

$$t_r = \frac{\epsilon_f}{\dot{\epsilon}_{cr}} \tag{2.10}$$

The constant ϵ_f gives the "creep ductility" or the strain at the onset of failure. The above equation assumes a constant stress during the creep test.
In case of varying stresses repeated in a cyclic manner an estimate of rupture time (or cycles to failure) can be made by using a special form of time-fraction rule, as given by Eq. 2.11.

$$N_f \left(\sum_{i=1}^{n} \frac{\Delta t_i}{t_{ri}} \right) = 1 \tag{2.11}$$

where,
N_f = number of repetitions or cycles to failure,
n = number of steps within a cycle,
Δt_i = time spent at stress level σ_i within a cycle, and
t_{ri} = rupture time for stress level σ_i.
Using Monkmann-Grant equality, Eq. 2.11 becomes

$$N_f \left(\frac{\sum_{i=1}^{n} \Delta t_i \dot{\epsilon}_{cri}}{\epsilon_f} \right) = 1 \tag{2.12}$$

Where $\dot{\epsilon}_{cri}$ is the steady state creep rate for stress level σ_i. Realizing that the numerator term within the summation sign is the creep strain accumulated during time Δt_i, the summation for all steps n within a cycle gives the Accumulated Creep Strain, ϵ_{acc} , for the whole cycle. Thus, the above Equation can be simplified as

$$N_f = \left(C^{'} \epsilon_{acc} \right)^{-1} \tag{2.13}$$

where, N_f = number of repetitions or cycles to failure, ϵ_{acc} = Accumulated creep strain per cycle, and $C^{'} = 1/\epsilon_f$, inverse of creep ductility. Notice that the strain exponent is -1 for this life prediction model.
Eq. 2.13 can also be derived using a fracture mechanics approach, as discussed previously in *Syed* 1997 [25]. It has also been shown by *Syed* 1997 [25], that this equation can easily be converted into energy density based life prediction model:

$$N_f = \left(W^{'} w_{acc} \right)^{-1} \tag{2.14}$$

[1]Some other types of constitutive relations have also been employed by *Syed* to establish life prediction model for SnPb and SAC, for further reading could be referred to [9] and [24].

where, N_f = number of repetitions or cycles to failure, w_{acc} = Accumulated creep energy density per cycle, and $W^{'}$ = Creep energy density for failure. Equations 2.13 and 2.14 give the cyclic creep, *Fatigue*, life due to varying and repeated stresses for a single creep mechanism.
Since a number of constitutive models are using the hyperbolic sin relationship, see Eq. 2.2, the same 12 data points for SAC solder were simulated using the same equation in ANSYS by *Syed*, and the accumulated creep strain and dissipated creep strain energy density were calculated for each case and the life prediction model parameters were determined using linear regression analysis. Again a good fit was found for the data and the mean life can be predicted by using the following equations:
using accumulated creep strain:

$$N_f = (0.0513\epsilon_{acc})^{-1} \tag{2.15}$$

using creep energy density:

$$N_f = (0.0019w_{acc})^{-1} \tag{2.16}$$

Syed has determined the constants, $C^{'}$ and $W^{'}$, for the double power law[1] as well.
Comparing above two life prediction models for double power law creep and hyperbolic constitutive equations, the exponents were determined as -1 for both accumulated creep strain and creep strain energy density. The values of constants, however, are slightly different. This difference is due to the actual values of creep strain and energy density calculated from two constitutive models. This shows that the life prediction model cannot be independent of deformation constants used to simulate the material behavior [24].

2.6.2 Schubert's approach and models

Schubert et al. 2003 [17], describe in detail the life-prediction models of SnPb(Ag) and SnAgCu solder joints for thermal cycle conditons. Their work deals with the effect of different solder interconnect alloys and the effect of different package types (PBGAs, CSPs, FlipChip on FR-4 with and without underfill) on the fatigue life, under different temperature cycling conditions.
According to [17] while considered solder alloys are above 0.5 of their melting point at -40 °C, creep processes are expected to dominate the deformation kinetics. Failure of solder joints is a complex sequence of possible failure mechanisms involving grain/phase coarsening, grain boundary sliding, matrix creep, microvoid formation and linking, resulting in crack initiation and crack propagation. In the case of SnAgCu solder joints, the damage accumulation process leads to much less coarsening of the microstructure.
In this work authors present life prediction approaches based on two damage parameters: creep strains accumulated in one thermal cycle and the viscoplastic strain energy density dissipated per cycle for both SnPb(Ag) and SnAgCu solder joints which are accurate within 2X of actual life measurements.
An empirical model has been used by the authors for a long time life prediction,

[1] $\dot{\epsilon} = B_1 \exp(\frac{-H}{kT})(\frac{\sigma}{E(T)})^{n_1} + B_2 \exp(\frac{-H}{kT})(\frac{\sigma}{E(T)})^{n_2}$ [23].

which assesses the amplitudes of the accumulated creep strain ϵ_{cr}^{acc} along the damage path for estimation of mean cycles to failure N_f by simple application of a "Coffin- Manson" type relation:

$$N_f = \theta_1 \left(\epsilon_{cr}^{acc}\right)^{-c_1} \tag{2.17}$$

ϵ_{cr}^{acc} is the actual minimum (or average) over the path of local maximum equivalent creep strain. Besides creep strain criteria, also creep strain energy based methods have been applied to determine the fatigue of solder joints. The equation is to be read in terms of viscoplastic energy density:

$$N_f = \theta_2 \left(\Delta W_{cr}^{acc}\right)^{-c_2} \tag{2.18}$$

where ΔW_{cr}^{acc} is the actual minimum (or average) over the path of local maximum of viscoplastic strain energy density, dissipated per cycle. That means, an approach similar to that for the equivalent creep strain was chosen with regard to the distribution pattern of the creep energy density: The local minimum (or average) of a band of maximum creep energy density crossing the volume of the solder joints is assumed to determine the critical cycle number. The viscoplastic strain energy density is defined as the summation of the scalar product of stress and inelastic strain increment tensors.
The corresponding constants for *Schubert et al.*'s life predintion model are presented in Table 2.8.

Table 2.8: Life prediction model constants by *Schubert* [17].

Solder alloy	θ_1	c_1	θ_2	c_2
SnPb(Ag)	0.69	1.8	210	1.2
SnAgCu	4.5	1.295	345	1.02

2.6.3 Spraul's approach and model

Spraul et al. 2007 [27], performed some tests on low temperature cofired ceramics (LTCC)[1] substrates to study the lifetime of flip-chip solder joints for this type of substrate.
By combining the experimental results with the computer simulation, they generated equations that permit the prediction of the lifetime of solder joints based on finite element method (FEM) simulations. These equations could be used to calculate the lifetime for similar flipchip interconnects. The two common approaches (strain-based or energy-based) for generating such equations are compared. Both approaches were capable of describing the experimental observations.
Equations 2.18 and 2.17 were implemented in this work, while they were not able to derive a model for SAC solder joints. First of all, the empirical formulas on which the lifetime models are based contain two parameters, thus at least two data points are necessary to build a model and only one lifetime was determined for SnAg4Cu0.5 solder joints. Additionally, the cracks in the metalization make it impossible to calculate the load that the temperature cycles cause on the solder joints. Consequently according to [27] it was not possible to derive a model

[1] LTCC technology is a low cost process for fabricating multi-layer ceramic structures [26].

for SnAg4Cu0.5 with the currently available data. The determined coefficients by the authors for SnPb are listed in Table 2.9.

Table 2.9: Life prediction model constants by *Spraul et al.* [27].

Solder alloy	θ_1	c_1	θ_2	c_2
Sn37Pb	537.15	1.0722	12.213	1.1361

2.7 Results

In the following subsections major achievements in the field of finite element analysis (FEA) and experimental procedures and microstructural analysis of solder joints for different packages by different researchers are presented. Finally, a summary table of the results, where the exact number of cycles to failure is available, is presented.

2.7.1 State of the art for FE-Analysis of lead-free solders

Vandevelde et al. 2007 [28], compared reliability of SnPb and SnAgCu solder. This comparison is based on non-linear finite element modelling. Three packages have been selected: silicon CSP, underfilled flip chip and QFN package. Also the effect of thermal cycling conditions has been investigated by these researchers. According to the results of their simulation, comparing the induced inelastic strains in the solder joint, the lead-free SnAgCu generally scores better thanks to the lower creep strain rate. On the other hand for the CSP and flip chip package, SnAgCu scores worse for the more extreme loading conditions when the inelastic dissipated energy density is selected as damage parameter. The main reason is that due to the lower creep strain rate, the stresses become higher for SnAgCu resulting in higher hysteresis loops with more dissipated energy per cycle. For the QFN package, SnAgCu scores much better.
For this work, the authors selected *Darveux*'s constitutive relation, Sec. 2.5.1 for SnPb , and *Wiese*'s equation, Sec. 2.5.9 for SnAgCu. For elastic modulus, the relation suggested by *Darveux et al.* [10] were used. A CTE value of 17.6 ppm/°C for SnAgCu and 25.5 ppm/°C for SnPb were implemented in this study.
Authors mention that the effect of plasticity is negligible [29] and they use creep as the only inelastic behavior. Moreover, there is no good plasticity data for SnAgCu in literature [10].
Fig. 2.2 shows the FEM model for the 5×4 mm CSP packasge. The structure is subjected to a uniform temperature cycling load and the results of the simulation are the induced deformation and stresses/strains.
For this CSP, the main deformation mode of the solder joint is shear between the stiff silicon chip (2.6 ppm/°C, 169 GPa, 0.68 mm thickness) and the FR4 board (16 ppm/°C, 25 GPa, 1 mm thickness). With this model, the one-to-one comparison is simulated for the two solder materials.

Table 2.10: Three loading conditions for FE-analysis by *Vandevelde et al.* [28].

ID	Range	Cycle time	Ramp-up	Dwell
LC1	0-100 °C	30 min	5 min	10 min
LC1	-40 to 100 °C	60 min	15 min	15 min

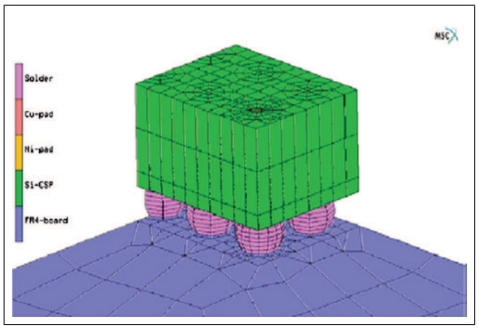

Figure 2.2: Three dimensional FEM for the 5 × 4 CSP mounted on a 1 mm thick FR4 board [28].

They performed simulation for two loading conditions, Table 2.10. It is expected that the trends can be dependent on the loading conditions. Considering the results, inelastic strain per cycle, averaged over damage volume, per thermal cycle were reported for all packages, for calculating life time. As depicted in Fig. 2.3 the inelastic energy is the area of this hysteresis loop.

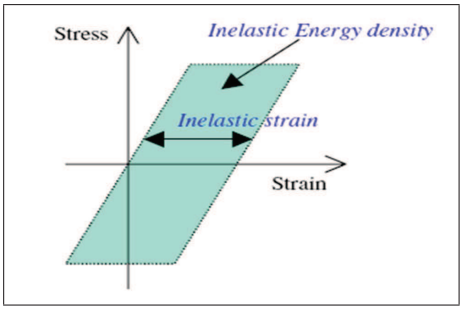

Figure 2.3: Schematic drawing explaining the difference between inelastic strain and inelastic strain energy density [28].

For SnAgCu, the stresses reach much higher values during the temperature cycling, resulting in higher hysteresis loops. Although the inelastic strain for SnAgCu during LC2 is smaller (= width of the loop), the dissipated energy per cycle (= area in the loop) is higher due to the higher stresses. Figs. 2.4 and 2.5 shows the hysteresis loops for one normal and one shear stress/strain component and proves the upper statement.

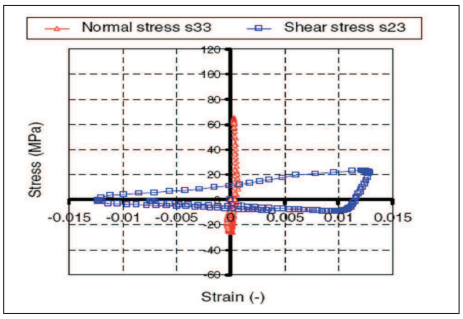

Figure 2.4: Hysteresis loop for one normal and one shear component for SnPb case [28].

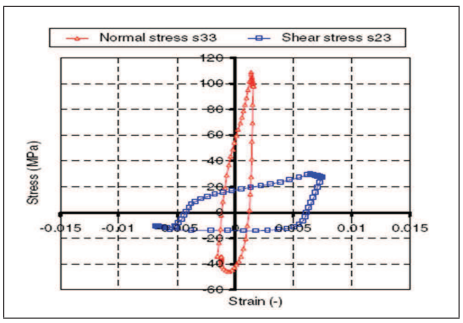

Figure 2.5: Hysteresis loop for one normal and one shear stress for SnAgCu case [28].

Comparing the induced inelastic strains, the lead-free SnAgCu generally scores better thanks to the lower creep strain rate. Table 2.11 shows the results of their simulation for all packages.

Table 2.11: Inelastic strain, averaged over damage volume, per thermal cycle for all packages by *Vandevelde* [28].

	0-100 °C			-40 to 100 °C		
Package	flip chip	CSP	QFN	flip chip	CSP	QFN
SnPb	1.41%	1.17%	0.44%	2.51%	2.08%	0.88%
SnAgCu	0.73%	0.43%	0.19%	1.59%	1.25%	0.19%
Pb/Pb-free	1.92	2.72	6.29	1.58	1.66	4.63

2.7.2 State of the art for experimental analysis

A combination of experimental and numerical work has been done by *Spraul et al.* 2007 [27], to asses the lifetime of flip-chip solder joints on low temperature cofired ceramics (LTCC), see Sec. 2.6.3. Their paper presents the results of an experimental study of the lifetime of flipchip solder joints on low temperature cofired ceramics (LTCC) substrates. To determine the actual lifetime of the solder joints, 54 substrates with two flipchips on each substrate, Fig. 2.6 were tested in temperature shock chambers. One half of the chips were soldered with SnPb37 solder, one half with SnAg4Cu0.5. The test conditions are listed in Table 2.12.

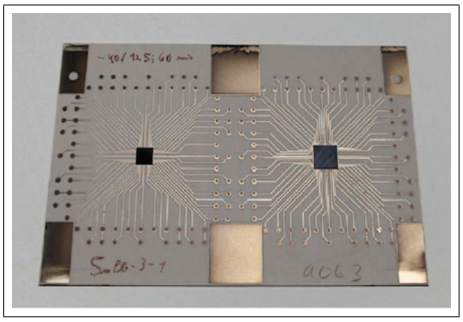

Figure 2.6: Test vehicle with two flipchips on a 152×102 mm2 LTCC substrate [27].

Table 2.12: List of parameters for temperature shock test by *Spraul* [27].

Condition	Test 1	Test 2	Test 3
Cold chamber (°)C	-40	-40	-40
Hot chamber (°)C	125	125	85
Hold time (min)	60	60	30

To identify joint failures, the resistance of the joints was measured regularly at room temperature. The mean lifetimes of the SnPb37 joints were depending on test condition and die size between 637 and 1465 temperature cycles. The failures occurred due to fatigue cracks in the solder, Fig. 2.7. The components soldered with SnAg4Cu0.5 solder showed a significantly longer time until electrical breakdown. A partial stress relief caused by cracks in the metalization layers was identified as one reason for the long time to failure of the lead free solder joints Fig. 2.8.

Finally, they derived a model for the lifetime prediction of SnPb37 joints based on FEM simulation from the experimental results. Both the accumulated creep strain (CoffinManson) based approach and energy-based approach were used. Both equations achieved a good approximation of the experimental observations. It must be noted that only four independent experiments were available for the determination of the coefficients of the lifetime equations, see Sec. 2.6.3.

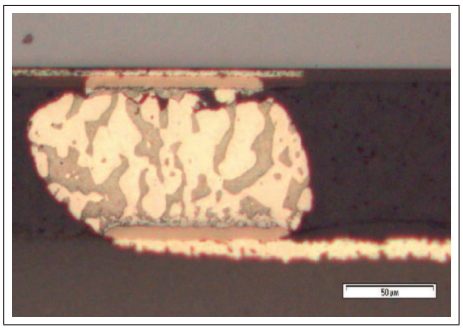

Figure 2.7: Metallographic section through a SnPb37 solder joint after 1000 temperature shock cycles, -40/125 °C, 60 min hold time. [27].

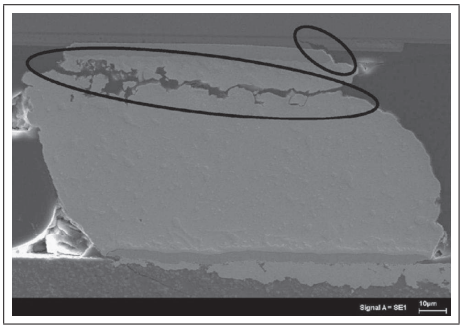

Figure 2.8: Section through a SnAgCu solder joint. Two cracks can be observed: A crack in the solder joint and a crack in the metallization layer of the flipchip [27].

Xia and *Xie* 2007 [3], examined the reliability of lead-free assemblies under thermal cycling for different types of surface finishes. Thin small package (TSOP) on FR4 PCB with Sn3.0Ag0.5Cu (wt%) solder was selected for this investigation. The profile of thermal cycling was in the range $0 - 100°C$ and the dwell time at the extreme temperature zone was 5 min. The ramp rate between the extreme temperatures was about $3 - 5°C$/min. The results of this work show that OSP finish reveals better performance than its ENIG counterparts. Crack originates at the fringe of heel fillet in both cases. The propagation of crack in the ENIG case is along the device/solder interface, ates at the fringe of hell fillet in both cases. The propagation of crack in the ENIG case is along the device/solder interface, while in the case of OSP, the crack extends parallel to the solder/PCB interface, Fig. 2.9. When the OSP finished are employed, many Cu_6Sn_5 precipitates from inside the bulk solder and have a strengthening effect on the solder joint, resulting in better reliability performance as compared to those with ENIG finishes.

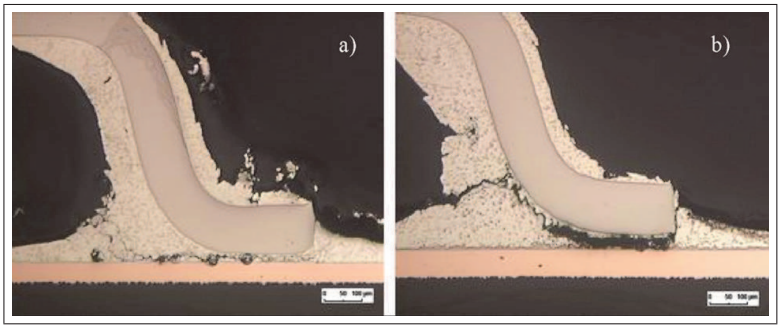

Figure 2.9: Typical cross-sectional optical images of samples after 7500 cycles, (a) OSP, (b) ENIG [3].

Sundelin et al. 2005 [30], performed some constant load creep tests using single-overlap shear specimens at 85 °C and 105 °C. Their test matrix included three different SnAgCu pastes with hypoeutectic, eutectic, and hypereutectic compositions. An Sn63Pb37 solder paste was used as a reference. The PCB finishes used were NiAu, organic solderability preservative (OSP) and immersion tin.
According to the results, the SnAgCu solder with eutectic or near-eutectic composition is the safest choice when the creep behavior of solder joints is considered. Of the three different PCB surface finishes, immersion tin is the most favorable choice for use with SnAgCu joints when creep is the predominant deformation mechanism in the joints. On the "NiAu" finish the creep properties of SnAgCu solder joints were significantly "weaker" in eutectic and hypereutectic SnAgCu joints than on Sn and OSP. The rupture time of the solder joints was determined for the various shear stresses and solder compositions. The final results are shown in Fig. 2.10 for 85 °C. A regression line was plotted for each solder/PCB finish combination.
The differences in creep properties between SnAgCu and SnPb solder joints are significant. Fracture occurred in the SnPb solder joints at about a 50-80% lower stress level than in SnAgCu joints for the same temperature and time to rupture. This was caused by the significantly higher homologous temperatures that the SnPb joints experienced at 85/105 °C; 0.785/0.829 Tm (homologous temperature) for SnPb and 0.731/0.771 Tm for the SnAgCu solders, respectively. Also the shear strength of SnPb solder is generally found to be lower than that of SnAgCu solders (*Nishiura et al.* 2002 [31], and *Li et al.* 2001 [32]), which decreases the creep resistance of SnPb solder joints compared to that of SnAgCu solder joints.
Nurmi et al. 2004 [5], performed thermal shock tests on two types of resistors, 0603 and 0405, by using three different compositions of lead-free solders: hypoeutectic 96.5Sn/3.0Ag/0.5Cu, eutectic 95.5Sn/3.8Ag/0.7Cu, and hypereutectic 95.5Sn/4.0Ag/0.5Cu. A eutectic SnPb solder was used as a reference. The test boards were temperature-cycled from $-40°C$ to $+125°C$ until all samples failed. Finally, they analysed the results of the temperature cycling test by using cross-sectioning of the failed joints and analyzing the fracture behavior and microstructures of the solder joints by using scanning electron and optical microscopy.

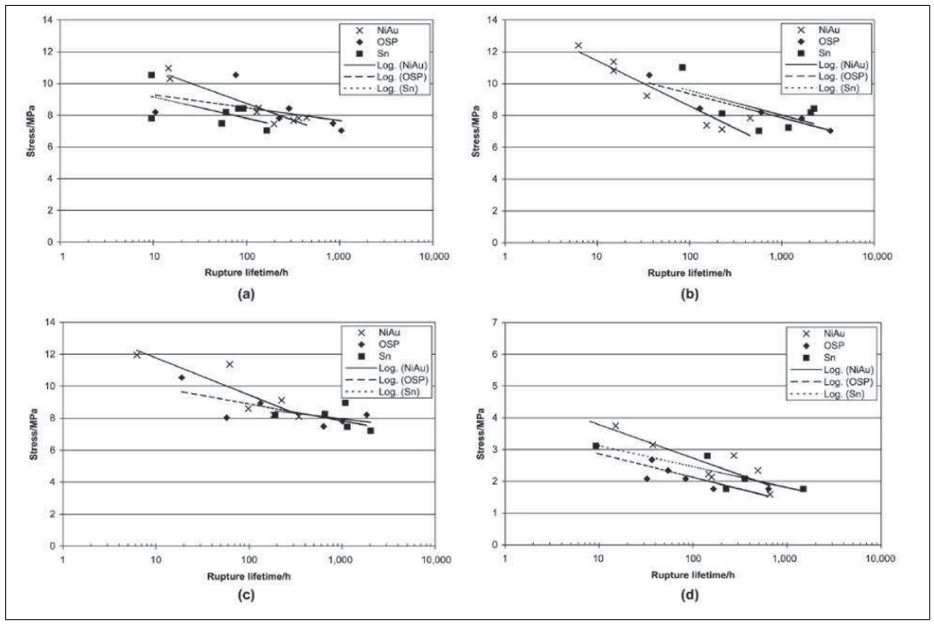

Figure 2.10: The creep test results at 85°C for (a) hypoeutectic SnAgCu; (b) eutectic SnAgCu; (c) hypereutectic SnAgCu; and (d) SnPb [30].

The results of their experiment suggest that the majority of the cracks in the SnAgCu joints initiated under the components, where the solder was the thinnest varying between 15 and 20 μm with both 0603 and 0402 resistors. This is shown in Fig. 2.11. In that thin section the strain caused by the mismatch of CTEs between the PCB, the solder and the component during the thermal shock test is the biggest leading to the initiation of a crack in the solder joint.

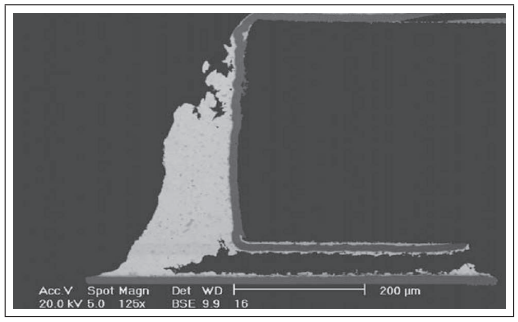

Figure 2.11: Crack initiation under the component metallization in eutectic SnAgCu solder joint [5].

The cracks propagated either through the fillet or by going upward vertically, as seen in Fig. 2.12, finally leading to a total failure of the joint. Vertical cracking was typical especially for the SnPb joints, where a Pb-rich phase formed a quite uniform layer next to the Ni_3Sn_4 intermetallic layer, and cracks propagated along the interface between the Pb-rich phase and the Sn matrix. This is illustrated in Fig. 2.13.

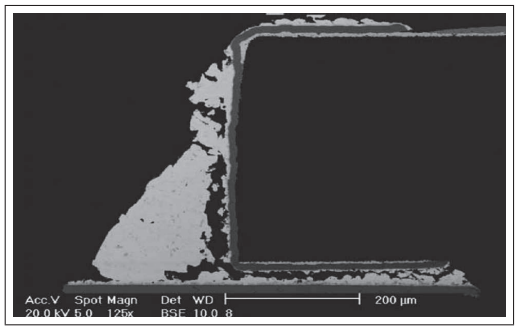

Figure 2.12: Cracking in both horizontal and vertical direction in the hypoeutectic SnAgCu joint [5].

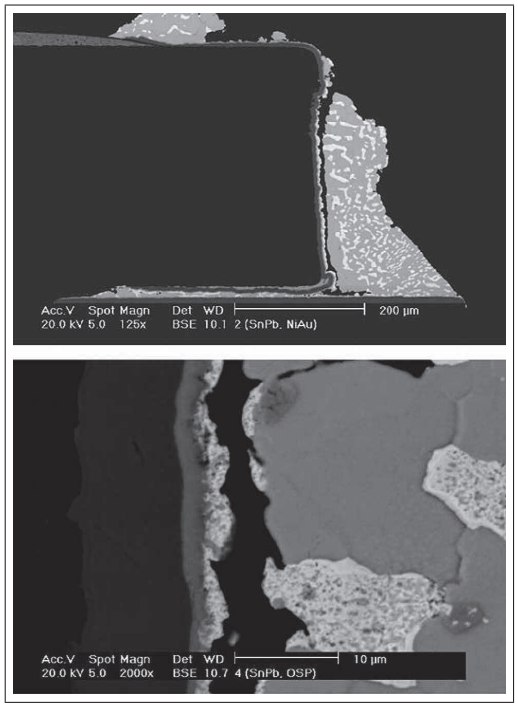

Figure 2.13: Crack propagation along the interface between the Pb rich phase and the Sn matrix in the SnPb solder joint [5].

In several SnPb joints the vertical cracking occurred even before the cracking under the component. This can be considered as a very potential reason for the significantly lower reliability of the SnPb joints compared to the SnAgCu joints, as the Pb rich phase makes the joints more vulnerable to cracking in an earlier stage of the thermal shock test. In both SnAgCu and SnPb joints the cracks initiated and propagated mostly in the solder joint, and only in some short stages the cracks propagated along the interface between the bulk solder and the intermetallic layer at either component's or PCB's side. At the

end researchers, mention that as a whole, the reliabilities of all lead-free solder joints were remarkably better than that of the tin-lead solder joints. This clearly indicates that the shift toward the lead-free electronics production should not be as great a concern as it used to be a couple of years ago, at least if electronics products are used in environments where only thermo mechanical stresses occur, see Table 2.13.
Ratchev et al. 2003 [33], studied two kinds of samples: Polymer Stud Grid Array packages soldered on a Printed Circuit Board (PCB) using either eutectic SnAgCu solder or a standard Sn62Pb36(Ag2) solder. In both samples a NiAu surface finish was present on the bond pads. The reliability of the solders was tested by means of thermal cycling in the range $-40°$C to $125°$C (1hour cycle time, air to air, 15 minutes dwell time). Authors did some failure analysis of both solders by means of cross-sectioning and Scanning Electron Microscopy (SEM) observation. Their reliability results show that the standard Sn-Pb-Ag solder has a much lower reliability than Sn-Ag-Cu solder when it is deformed to high strain (3.9 times lower N_{50}). The reason for this is a brittle fracture mode at the UBM interface of the Sn-Pb-Ag joint, see Fig. 2.14.

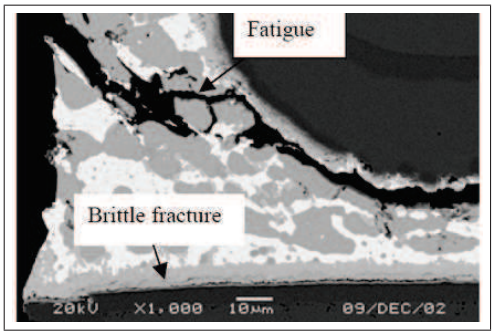

Figure 2.14: Corner Sn-Pb-Ag solder connection, high strain, failed after 1600 cycles (cycled till 5400 cycles) Two different failure modes are present solder fatigue and brittle interface fracture [33].

The continuous layer of the brittle $(Au, Ni)Sn_4$ intermetallic, formed during the thermal cycling of the SnPbAg solder, which is responsible for the brittle fracture mode, did not form when the Pb-free solder was used. Actually, the same intermetallics form at the UBM interface, but not as a continuous layer. One reason for this is that a significant amount of the Au, dissolved in the solder, precipitates in the bulk as $(Au, Ni)Sn_4$ particles, which naturally reduces the amount of this phase formed at the interface. Therefore a continuous layer of the brittle $(Au, Ni)Sn_4$ intermetallic can not be formed at the interface, see Fig. 2.15. Consequently, under the same conditions, the brittle fracture mode is less dangerous for the Sn-Ag-Cu than for the Sn-Pb-Ag solder.

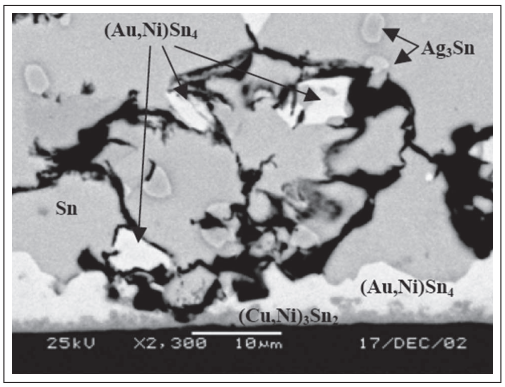

Figure 2.15: Cracks form at brittle $(Au, Ni)Sn_4$ particles in the volume. No brittle fracture occurs at the interface with the UBM because the brittle $(Au, Ni)Sn_4$ phase does not form a continuous layer. A thin, but very stable $(Cu, Ni)_3Sn_2$ phase forms at the interface [33].

Considering the microstructure, the major difference between both solders is that many particles of the brittle $(Au, Ni)Sn_4$ intermetallic are spread in the volume of the Sn-Ag-Cu solder. This leads to a specific type of solder fatigue, which they named *web-like*. The difference, compared to the normal solder fatigue, is that the crack propagates through the bulk of the solder in a web-like way linking the brittle Au-containing particles. This propagation mechanism is certainly beneficial for the joint reliability, because it deviates the crack from the shortest way of development and slows down the propagation kinetics. Those two effects are illustrated in figs. 2.16 and 2.17. Summarizing, not only the lack of the brittle fracture mode, but also the specific solder fatigue mode, contribute to the higher reliability of the Sn-Ag-Cu solder compared to the traditional Sn-Pb-Ag.

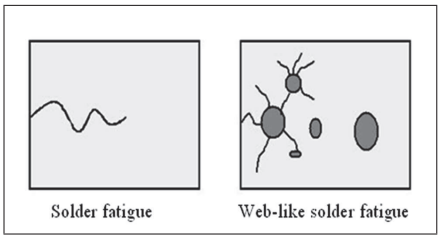

Figure 2.16: Web-like solder fatigue deviates the crack from the shortest way of propagation [33].

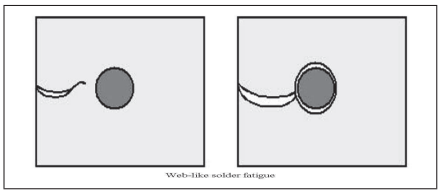

Figure 2.17: The speed of crack propagation is related to the sharpness of the crack, which decreases every time it meets a particle. [33].

Stam and Davitt 2001 [1], performed accelerated reliability tests on 1206 resistors using both SnAg3.8Cu0.7 and Sn62PbAg2. Thermal shock test in the range $-20°C$ to $+125°C$ and 3 min dwell time used by these authors. They performed a random vibration test in addition to the thermal shock test.
According to their results, dependent on the board and component metallizations and use environment, the reliability of the lead-free solders could perform better or worse than the lead based solders, so there is significant difference between lead bearing and SAC solders in fatigue resistance, but it is influenced by the package type and board metallization.
It is also mentioned that SAC performs better on immersion-Ag or OSP-Cu surface finish.
Xie et al. 2002 [34], studied the reliability of chip scale package (CSP) using lead-free solder. Effects of using different PCB surface finish, and reflow process were investigate. Two commonly used PCB surface finishes were employed: organic solderability preservative (OSP) and electroless nickel immersion gold (ENIG). From the results of thermal cycling test, it is learnt that all CSPs tested are qualified for consumer products application but only CSP24 and CSP308 can meet the requirement of telecomm applications. Compared to ENIG, OSP is more reliable as PCB surface finish in both thermal cycling and thermal shock tests. The reliability is affected not also by the pick of the temperature but also by the dwell time. The optimum setting would be different when using ENIG or OSP finishes.
For their test, the PCB was made from FR-4 with double sided and coated with electroless nickel and immersion gold (ENIG) or organic solderability preservative (OSP). SAC alloy, 95.5Sn/3.9Ag/0.6Cu, had been selected and a commercial solder paste with no-clead, resin-based and low activity flux was used in their experiment. Two types of temperature cycling tests, thermal cycling (TC) and thermal shock (TS), were used to evaluate the reliability. In the reliability tests, only 3040 cycles were performed in the thermal cycling and 500 cycles were completed in thermal shock. For thermal cycling, both real-time monitoring and offline testing are used. For thermal shock, only offilne probing was done. The test procedure of *Xie et al.* follows IPC-9701 and the failure definition criteria is 20% resistance change.
From results ofthermal cycling test, only CSP24, CSP308 and QFP208 can meet the telecomm application requirement by IPC-9701. From results of thermal shock test, only USMD using ENIG finished PCB and CSP24 using OSP finished PCB could not meet the telecomm specification by IPC-9701. Overall, OSP outperformed ENIG as PCB surface finish for lead-free process.

2.7.3 Results of reliability analysis

In a number of published papers the number of life cycles to failure for different components have been mentioned explicitly. These results are based on either simulations and experiments together. Where there is no number means that no prediction for life cycles was done or it was impossible for the corresponding authors to draw a conclusion based on their experiment.

2.8 Conclusions

SnAgCu is more creep resistant than SnPb, this makes this solder stronger when creep in the main deformation mechanism. It is well documented in the literature that when solder works at high homologous temperture, around 0.5, creep dominates the deformation kinetics. Since, SnPb has lower melting point it is less creep resistant than SAC.
No overal conclusion regarding the reliability of solder joint using SAC, has been made yet, instead reliability analysis is done case by case for each package for a certain type of loading, using thermal shock test or other types of test considering loading condition.

Table 2.13: Summary table of reliability analysis results

Ref.	Package/ PCB surface finish	Test condition Range (°C) and Period (min)	Solder	MTTF Cycles(C) Years(Y)	Num. of cycles to 1% failure	FIT
[17]	PBGA-272/NiAu	-40 to 150 / 44	SnPb	2814 (C)		
[37]	PBGA-272/NiAu	-40 to 125 / 60	SnPb	5560(C)		
[36]	PBGA-256/OSP	-40 to 125 / 60	SnPb	3798(C)		
			SAC	8083		
[34]	QFP208/ENIG	0 to 100 / 30	Sn95.5Ag3.9Cu0.6	381(Y)		300(Y)
	QFP208/OSP			381		300
	USMD8/ENIG			53.2		2147
	USMD8/OSP			49		2330
	CSP24/ENIG			381		300
	CSP24/OSP			381		300
	CCSP224/ENIG			45.4		2514
	CCSP224/OSP			63.9		1786
	CSP308/ENIG			106.8		1068
	CSP308/OSP			224.1		509
	QFP208/ENIG	-55 to 125 / 11				1249(Y)
	QFP208/OSP					727
	USMD8/ENIG					2204
	USMD8/OSP					727
	CSP24/ENIG					727
	CSP24/OSP					2146
	CCSP224/ENIG					727
	CCSP224/OSP					727
	CSP308/ENIG					727
	CSP308/OSP					727
[27]	flip chips/LTCC	-40 to 125 / 30	SnPb	749(C)		
	10×10 mm^{2}die					
	7×7			1465		
	10×10	-40 to 125 / 60		637		
	10×10	-40 to 85 / 30		1328		
	10×10	-40 to 125 / 30	SnAgCu	1611		
	7×7			2%failure after 1500 cycles		
	10×10	-40 to 125 / 60		3%failure after 1000 cycles		
	10×10	-40 to 85 / 30		0%failure after 1500 cycles		
[5]	0402/NiAu	-40 to 125 / 30	SnPb	2338(C)		
	0402/OSP			3082		
	0402/NiAu		95.5Sn3.8Ag0.7Cu	3328		
	0402/OSP			3244		
	0603/NiAu		SnPb	1651		
	0603/OSP			1521		
	0603/NiAu		95.5Sn3.8Ag0.7Cu	2590		
	0603/OSP			2929		
	0402/NiAu		SnPb		997	
	0402/OSP				1571	
	0402/NiAu		95.5Sn3.8Ag0.7Cu		2094	
	0402/OSP				2129	
	0603/NiAu		SnPb		1052	
	0603/OSP				711	
	0603/NiAu		95.5Sn3.8Ag0.7Cu		1373	
	0603/OSP				698	

Chapter 3

Implementations

3.1 Overview

The main objective of this work was to perform Finite Element Analysis (FEA) to simulate creep deformation according to a suitable constitutive relation, then use the result of this simulation; accumulated creep strain during one cycle, and implement one life-prediction relation to predict the number of life cycle to failure. Moreover, a thermal shock experiment was designed to evaluate the reliability of both SnPb and SnAgCu. In the following sections, the requirements of FE-analysis for thermal simulation of SwissCube's Mother Board (MB) , as the most important board with specific features, two dimensional simulation of creep deformation of solder joints for an 0805 resistor, three dimensional simulation of creep deformation of solder joints for a D-Pack MP725 film resistor, and finally the requirements for experimental analysis of solder joints are presented.

3.2 Thermal simulation of MB

The temperature fluctuation outside SwissCube is simulated with a sin function. Every 90 min satellite rotates once in its orbit, 60 min in the day light and 30 min in the eclipse. As an estimation, it is supposed that the duration of the day-light and eclipse time are equal to 45 min and each cycle takes 90 min totally.
The temperature of the environment in the space fluctuates in the range -50°C to 70°C . To simulate temperature variation of the board with respect to time some other assumptions are required to be made.

3.2.1 Geometry

The geometry of the board is considered according to the latest version of the mechanical plans [38]. This geometry is used to prepare a three dimensional model in ABAQUS Standard 6.5. On the MB there are three locations where dissipation systems are assembled. These dissipation systems are used to dissipate the excess of power generated by solar cells (in the light) or maintain a minimal temperature in the shadow (eclipse) by using the energy of the batteries. The three assemblies will be located near the corners of the MB [38], but

the final location of the resistors and transistors have not been defined for the moment. This system is the unique feature of the MB and that is why there is an special interest to simulate temperature variation for this board.
The contact areas of MB and frame is also simulated considering the thickness of the frame in these areas. This needs to be taken in to account that this simulation is valid until there is no side contact between board and frame, moreover the area of the contact is important.

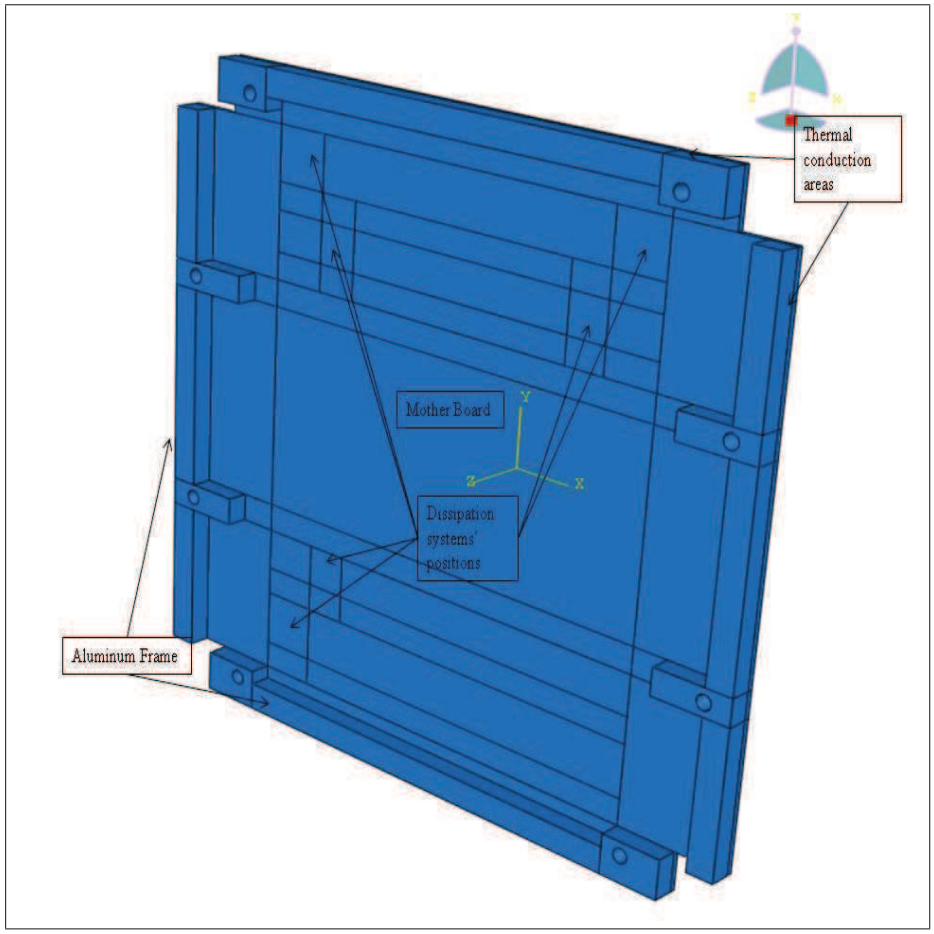

Figure 3.1: 3-Dim. model of MB (98×96×0.8 mm) and frame (thickness = 3 mm), holes are used to employ screws, on dissipation systems' positions a constant surface heat fluxes were applied.

3.2.2 Material properties

MB is made of FR-4 epoxy composite laminate with several copper layers. Frame is made of Aluminum 7075-T73 [38] .The corresponding properties of PCB substrate are given in Table 3.1.

Table 3.1: FR-4 properties [42, 38].

Material	Density (g/cm^3)	Coefficient of thermal expansion (CTE) ppm/K	Thermal conductivity $Wm^{-1}K^{-1}$	Specific heat $JKg^{-1}K^{-1}$
FR-4	2.0	14 (in-plane)	0.62	950
Al 7075-T73	2.81	24.5	150	960
Copper	8.81	16.9	391.1	385

To calculate material properties especially thermal conductivity it is assumed that 12.5% of the board is made of copper and the material properties is obtained by calculating the wighted average of thermal conductivity of copper and FR-4 according to their thickness. For example, for thermal conductivity we have:

$$TC = \frac{(TC)_{copper} \times (copper's\ \ thickness) + (TC)_{FR4} \times (FR-4's\ \ thickness)}{(copper's\ \ thickness) + (FR-4's\ \ thickness)} \tag{3.1}$$

This approach is chosen since there is no doable way to determine the properties exactly.

3.2.3 Boundary conditions

In the space there is no air, so there is no heat transfer by convection or conduction. Heat is transferred to the outside through the Al-frame from mother board, and Al-frame exchanges heat to the outside by radiation. According to the provided information, outside temperature changes from -50 °C to +70 °C, while heat transfer by radiation depends on the 4^{th} order of temperature, and emissivity as well[1] [39]. All these makes it very difficult to determine the variation function excatly, a good assumption would be to estimate temperature variation with a *sin* function with 90 min period, equal to the satellite's period, and an amplitude which is equal to the half of the temperature range, +60 °C, see Eq. 3.2.

$$T(t) = A_0 + Asin(\omega t) \tag{3.2}$$

where $T(t)$ is the temperature in Kelvin, $A_0 = 283.15$ in Kelvin, $A = 60$, and $\omega = 0.0011633$, and t is time in second. In Fig. 3.1, dissipation systems are also demonstrated. The dissipation system is made of 3 same assemblies. These three assemblies will be located near the corners of the MB. For DS, the worst case is when the batteries are fully charged (so they are not able to receive more energy) and when the subsystems consume nothing. In this case, all the power generated by the solar cells will be dissipated on one MB. Every DS assembely dissipates a third of the total power, and maximum dissipated power will be 3 Watts totally. One assembly is made of two components : 1 resistor and 1 transistor. For thermal analysis it was assumed that 0.5 Watt is dissipated on the resistor and the same value on the transistor.

[1] $Q = \epsilon \cdot \sigma \cdot A \cdot T^4$, ϵ is emissivity, σ is Stefan-Boltzman constant, A is area and T is temperature.

The D-Pak (DS) as a pad is placed on the bottom face in order to increase the thermal conduction with the PCB. This pad is welded on the PCB. So it was assumed that for each component 0.5W goes through its pad and pins [38]. A surface heat flux was applied uniformly on those areas, and it was assumed these dissipation systems are producing a constant surface heat flux during each cycle to have the maximum produced temperature.

3.3 2-Dimensional modeling of creep

Modeling is a useful tool used to supplement or replace accelerated tests, particularly in the early design stages. The modeling discussed here applies to creep induced ductile fracture only, and so will be suitable for modeling the damage that occurs due to typical thermal cycling of solder joints. The constitutive law plus fatigue law class of methods (encompassing FEA) are very popular, providing more accurate predictions with fewer restrictions than analytical methods, however, with increased set up time and computational cost [40]. Main objective is to model creep deformation considering it as the most important damage mechanism influencing solder reliability due to thermal cycling loads. For this work, one of the frequently used packages has been chosen to model creep deformation. This simulation is carried out in two dimensions thanks to the symmetry of the component and a uniform cross-section through the thickness of the package.

3.3.1 Geometry

Geometry of the model is presented in Fig. 3.2, the dimension of the land pattern for an 0805 resistor and the thickness of the solder is taken from [41].

3.3.2 Material properties

FR-4, package, and copper-layer are considered elastic materials just with elastic time-independent properties, and the only material with time-dependent properties is solder. FR-4's properties are considered the same as previous section, package is supposed to be made of alumina(Al_2O_3), and copper-layer's properties will be the extracted from [42], Table 3.2.

Table 3.2: Material properties for 2-Dim. FE-analysis

Material	Coefficient of thermal expansion (CTE) (m/m-°C)	Elastic modulus (E) (GPa)	Poisson ratio ν
FR-4	18.5	22	0.28
Copper	17	76	0.35
Alumina	3.9 @ -55 °C and 6.7 @ 100 °C	303	0.21

Solder is considered as an inelastic material with time and temperature dependent behavior, however only creep is considered as the main deformation mechanism. At first it is desired to have a value or relation for elastic modulus

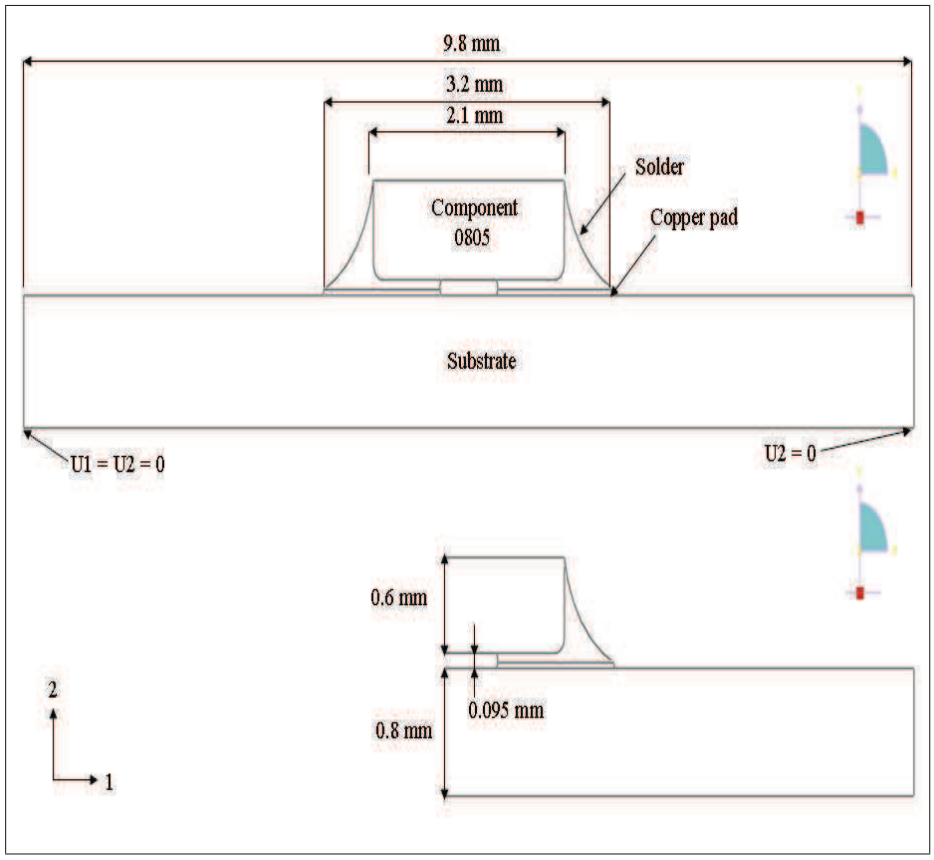

Figure 3.2: 2-Dim. model of 0805 resistor, copper pad's thickness is 0.035 mm.

of both solders; SnPb and SnAgCu. In different references there are different values and relations for calculating elastic modulus. For SnAgCu firstly, values or relations of elastic modulus from each reference are implemented with the corresponding constitutive relation, secondly, an average value of elastic modulus and a new constitutive equation which is obtained by fitting to other equations are employed.
For SnPb the same approach is followed, but the most conservative result[1] is taken into account for final comparison, and used for 3-dimensional analysis in the following.
To proceed further a comparison of the constitutive equations for SnAgCu is done by plotting creep strain rate evolution versus stress in the average temperature , see Sec. 2.5 for details on constitutive relations. Where the constitutive relation was not available in the tensile form, the constituive equation was transformed to the tensile form using Eq. 2.5 and Eq. 2.6, then all avilable constitutive relations from [15, 16, 17, 21, 18, 22, 20, 23] are plotted for different stresses at 283.15 K, Fig. 3.3.

[1]The boundary relations are always neglected.

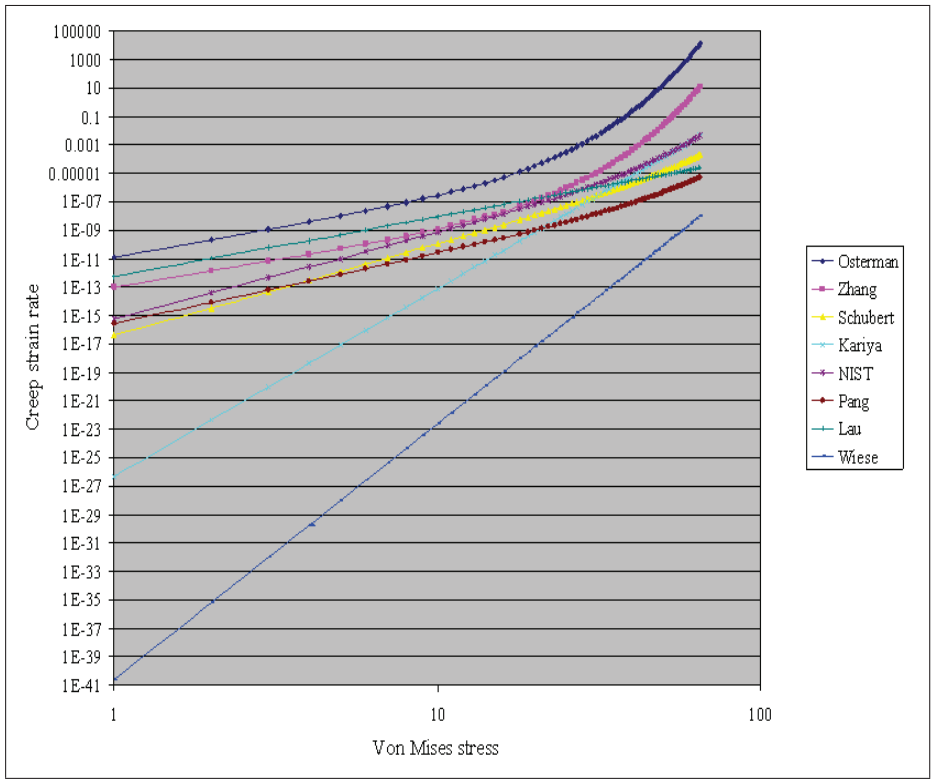

Figure 3.3: Creep strain rate is plotted versus equivalent stress for all mentioned constitutive equations for SnAgCu at T = 283.15 K.

As it is clear in the figure some creep relations have been developed either for low stress or for high stress regions. It is desired to have the safest assumption for the predicting number of life cycles to failure it means creep strain should reach to a high value, while it should be also possible to implement such a relation in ABAQUS. The procedure of choosing a suitable relation includes calculating a reasonable activation energy and fit a *sinh* function to the available constitutive relations. As a result in the following, *Osterman*'s, *Zhang*'s, *Lau*'s, and *Wiese*'s constitutive relations are not considered, since it seems they cover a small range of stresses and out of those regions, predict a very high or low creep strain.
Activation energy for *Schubert, NIST, Pang,* and *Lau*'s model are listed in Table 3.3, and for the new constitutive relation an average of these values are used.

Table 3.3: Activation energy for SnAgCu for different constitutive relations and the average value for the new relation.

Relation	*Schubert*	*NIST*	*Pang*	*Lau*	New
Activation energy (J/mole)	62916.7	67900	45200	44998	55253.675

Considering the general form of *sinh* constitutive relations, Sec. 2.5, there are three other values to be determined: power law multiplier or A, hyperbolic law multiplier or α, and stress order or n. By fitting a new equation to the selected

constitutive relations, a new *sinh* is presented, Eq. 3.3, the corresponding plot is presented in the next figure, Fig. 3.4.

$$\dot{\epsilon} = 3500\left[\sinh\left(0.05\cdot\sigma\right)\right]^{4.2} e^{-\frac{55253.675}{RT}} \tag{3.3}$$

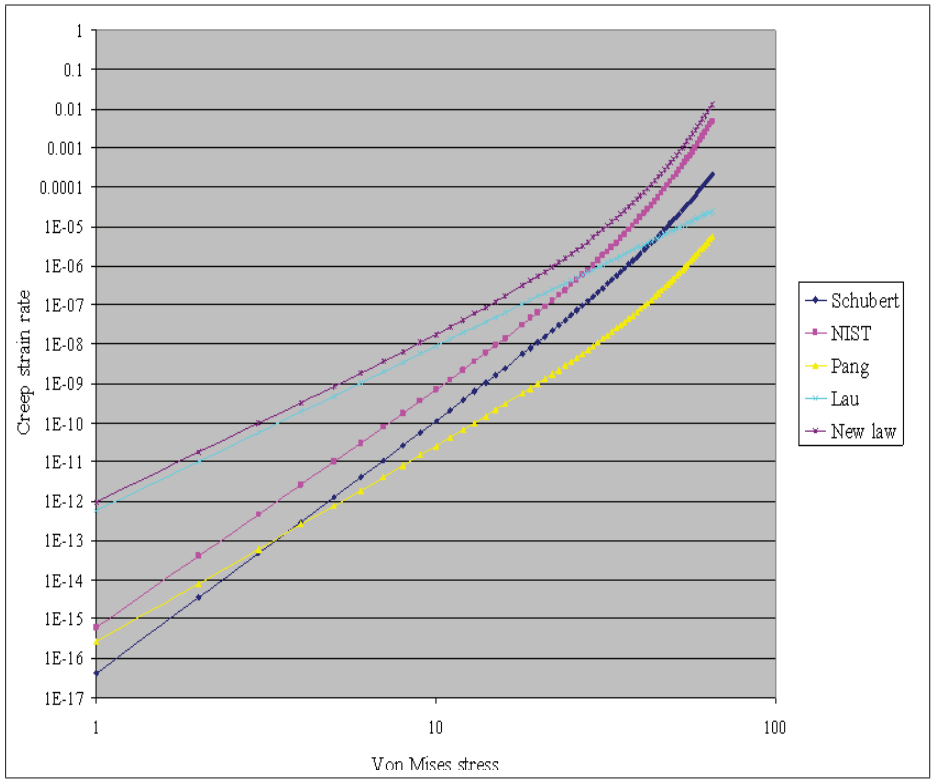

Figure 3.4: New constitutive relation in compare to other selected constitutive relations.

It is expected that calculating creep strain according to this new relation gives a lower value in compare to other selected constitutive relations.
For SnPb all aforementioned constitutive relations are implemented in 2-dim. FE-analysis. Elastic modulus changes linearly with time, [15, 16, 17, 21, 18, 22, 20, 23, 28], where the value was not in the same range as other values it was neglected, and an average of other valuse was used. Different researchers have used different relations for elastic modulus, Table 3.4, neglecting the relation used by *Zhang et al.* [16], and taking the average from others, a new linear relation for elastic modulus, Eq. 3.4, would be used along with new constitutive relation for SnAgCu.

$$E(MPa) = 74674 - 88.77 \times T(K) \tag{3.4}$$

Table 3.4: Elastic modulus for SnAgCu from [15, 16, 17, 21, 18, 28].

	Elastic modulus (MPa)					
T (K)	*Osterman*	*Zhang*	*Vandevelde*	*Kariya*	*Lau*	*Schubert*
223.15	50597.14	24219.4	62052.5	51763.65	53004	56909.65
348.15	50595.72	24216.83	37921.25	38138.65	52994	39197.15

3.3.3 Boundary conditions and loads

A uniform temperature which was obtained by first analysis, Sec. 4.2, was applied as a field in ABAQUS Standard 6.5, to the whole model. First analysis suggests that maximum temperature will not exceed 78 °C, and temperature varies with a *sin* function analogous to the thermal simulation, see Sec. 3.2.3. the cross section of the whole assembly and a part of the PCB which corresponds to the designed experiment, see Sec. 3.5 was modeled, and it was assumed that there are two displacement boundary conditions on two lower corners of the PCB, see Fig. 3.2.

3.4 3-Dimensional modeling of solders

For 3-dimensional analysis of solder joints one of the most important packages in terms of its function, has been chosen. Moreover, it is desired to compare the induced creep strain for a big but not stiffer package in compare to one of the smallest components, 0805 resistor. On mother board there are three dissipation systems, and each one includes one MP725 surface mount film resistor, Fig. 3.5 [43], which is chosen for 3-Dimensinal simulation.

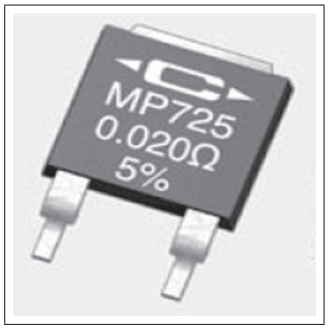

Figure 3.5: MP725 surface mount film resistor [43].

3.4.1 Geometry

To model this package, Fig. 3.5, it is more practical to use a CAD software then export the model to ABAQUS to perform simulation and FE-analysis. A 3-dimensional model of each part: front solder joints, end solder joint, heat sink[1],

[1]That is a metallic part under the package to increase heat transfer.

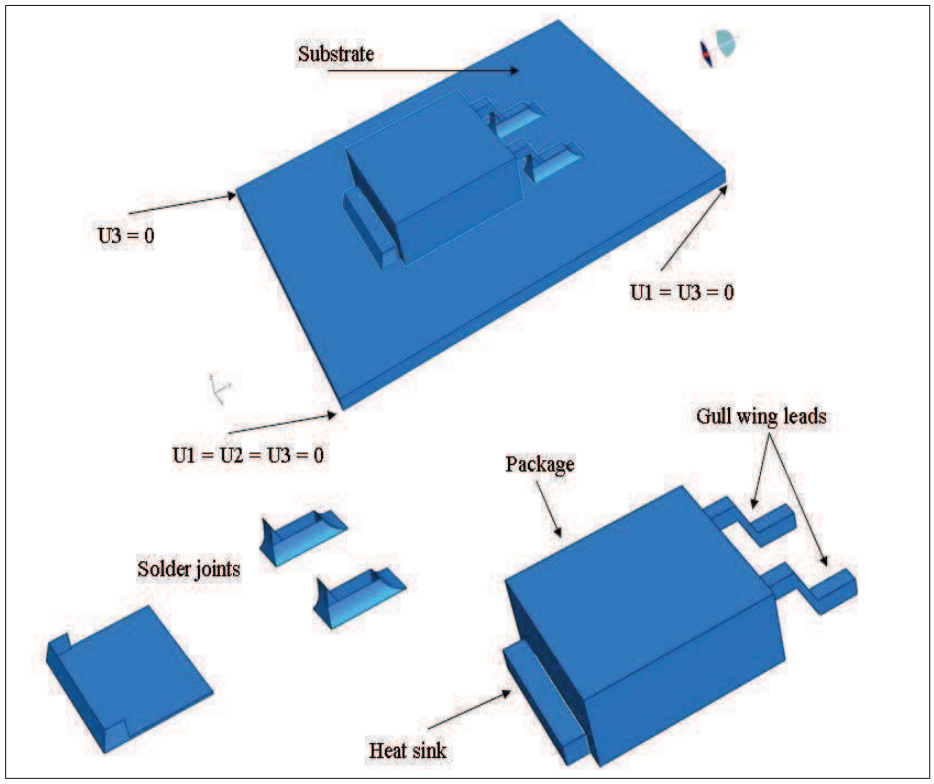

Figure 3.6: 3-Dimensional model of the MP725 surface mount resistor, displacement boundary conditions are shown by U.

package, and a part of the PCB substrate, was drawn by CATIA V5R15 and then the parts were exported to ABAQUS 6.7 in the step format[1], and assembled together to create the final geometry, Fig. 3.6. It is worthwhile to mention that in this model there are a lot of contact surfaces where parts are attached together,, , so *Tie* constraints should be used to attach these surfaces, however doing this in ABAQUS 6.5 created some problems, while using ABAQUS 6.7 solved this problem.

3.4.2 Material properties

No information is provided by the manufacturer or other resources regarding material properties of the package, however some tests show that it is made of a very stiff plastic, so the corresponding material properties are extracted from [42], considering a very stiff epoxy composite with a very high CTE to make sure stresses/strains reach to the highest value . Gull wing leads and heat sink are supposed to be made of copper, to have a very high conductivity Table 3.5, either for electricity or for heat. also because there is no other available information about these parts. PCB substrate have the same properties as before, see Sec. 3.2.2. For modeling solder's behavior the newly developed constitutive

[1]A standard type of exchange file between two softwares.

Table 3.5: Material properties for 3-dimensional simulation [42].

Material	CTE	Elastic modulus (GPa)	Poisson's Ratio
Epoxy	110	5.08	0.3

equation for SnAgCu, and the safest relation for SnPb are used, further details will be discussed in the next chapter.

3.4.3 Boundary conditions and loads

This is supposed that only thermal loads are present and the boundary conditions prevent the model to rotate or move rigidly, while they do not create a lot of stress concentration in the model. It must be noted as solid elements are finally used to perform FE-analysis the boundary conditions should forbid translations, only at three corner points, although its possible to choose other points, however , to let the model to freely expand or shrink while bending is also taken into account.

3.5 Experimental procedure

To assess reliability of SMT[1]assemblies, accelerated life tests (ALT) such as thermal cycling (TC) and thermal shock (TS)have been used for tin-lead solder joints for many years. Certain criteria should be met for different products according to different standards. For example, 500 cycles from -55 °C to 125 °C is the minimum requirement for telecommunication components in Bellcore standards, TR-NWT-000357 to ensure the reliability of product life [34].
However, due to time constraint, lack of some resources, and our special application, it was not possible or necessary to follow such a standard procedure, instead, a certain type of cycle which guarantees reaching to the maximum temperature was considered.

3.5.1 Test vehicle preparation

As mentioned before, two types of components were chosen to be tested using thermal shock test; 0805 resistor and MP725 film resistor. Two types of test vehicle were designed for this test, see Fig. 3.7[2], there are one hundered 0805 resistors on the resistor's board[3], and four dissipation systems which includes four MP725 on the other board.

[1]Surface mount technology (SMT) is a method for constructing electronic circuits in which the components (SMC, or Surface Mounted Components) are mounted directly onto the surface of printed circuit boards (PCBs) [45].

[2]See Appendix A for PCB layouts.

[3]Each resistor has a 2.7 Ohms resistance.

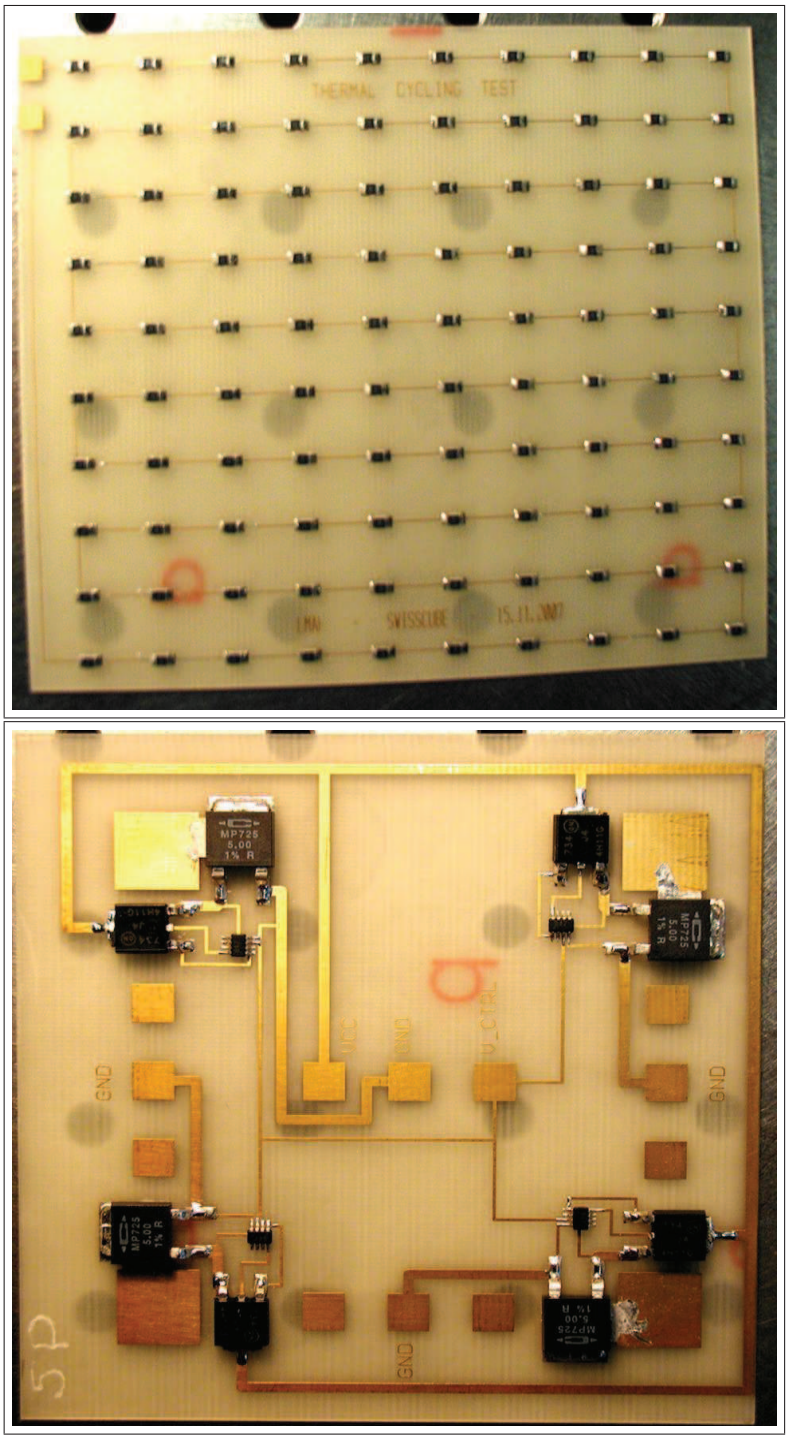

Figure 3.7: Two test vehicles have been designed for thermal shock test.

3.5.2 Test procedure

The experiment was carried out in a two-zone temperature shock chamber[1]. The nominal transfer time between the hot and the cold chamber was 10 seconds, and hold time (dwell) was 10 min in each chamber[2], so the total test cycle would be 20 min. For FE-analysis of solder joints test cycle's duration were considered 20 min.
Temperatures were measured every 10 seconds in the middle of one board for small resistors' (0805 resistor) board and beside the big resistor (MP725 film resistor) on the dissipation systems' board.
Moreover, using an external resistor, 180 Ohm, outside the oven in series with the circuits the continuity of the circuits' voltages were monitored. If one circuit had a cut then the voltage of this external resistor would drop to 0 Volts.

[1] Figures are available in Appendix B.

[2] According to the information [38] boards' temperature will reach to the maximum +70 °C and -50 °C in less than 10 min.

Chapter 4

Results

4.1 Overview

In the following sections, results of FE-analysis of temperature variation in mother board (MB), 2-dimensional and 3-dimensional FE-analysis of creep deformation in solder joints, life prediction results using aforesaid equations, see Sec. 2.6, and the results of microstructural analysis of solder joints after thermal shock test are presented.

4.2 Thermal simulation of MB

The main result from thermal simulation is the temperature variation, and estimating the maximum temperature and it's position on the board. To obtain maximum temperature, dissipation systems are considered to work constantly during each cycle as mentioned in Sec. 3.2.3. Since, there is no complex nonlinear effects, it was not expected to see a difference between linear and quadratic elements. First analysis was performed using both 4-node linear heat transfer tetrahedron (DC3D4) and 10-node quadratic heat transfer tetrahedron elements (DC3D10). The results slightly differs in terms of value and calculation time, so in the following quadratic elements were used to perform the rest of calculations. The maximum temperature was found to be in the center of one dissipation systems, necessary to repeat, that dissipation systems are modeled as a type of load; surface heat flux.
In Fig. 4.1, the results of simulation plus maximum and minimum temperatures, and their positions are presented, these maximum values are the biggest values during 3 cycles.
Simulation shows that temperature reaches to a stable value after one cycle, using temperature variation in the center of the MB as a reference, so, it is not necessary to simulate more than three cycles. Moreover the maximum temperature is achieved in the center of dissipation system. A comparison plot of the temperature in the dissipation system's (DS) center and MB's center is demonstrated in Fig. 4.2. Maximum temperature values for different locations on the mother board is given in Table 4.1, and a plot of the temperature evolution along the board's section are presented in Fig. 4.3. A comparison study has been also performed to assess the effect of changing material properties on the

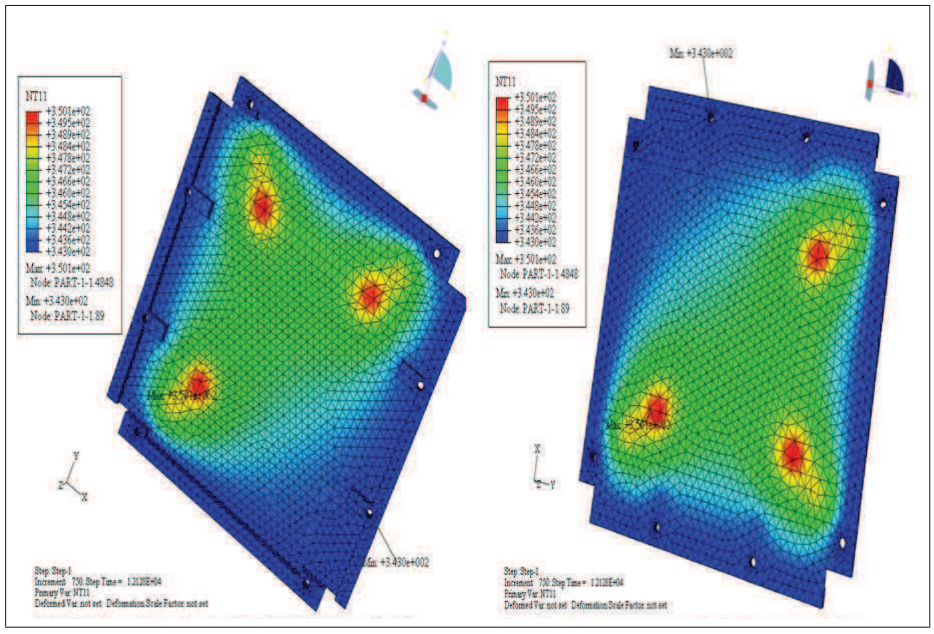

Figure 4.1: Thermal simulation results of mother board's (MB) 3-dimensional model, the max and min and temperature positions are displayed.

maximum and minimum temperature for DS's center, these results show that having copper is the most important factor in reducing temperature variations and maximum temperature, for a complete review see Appendix C.

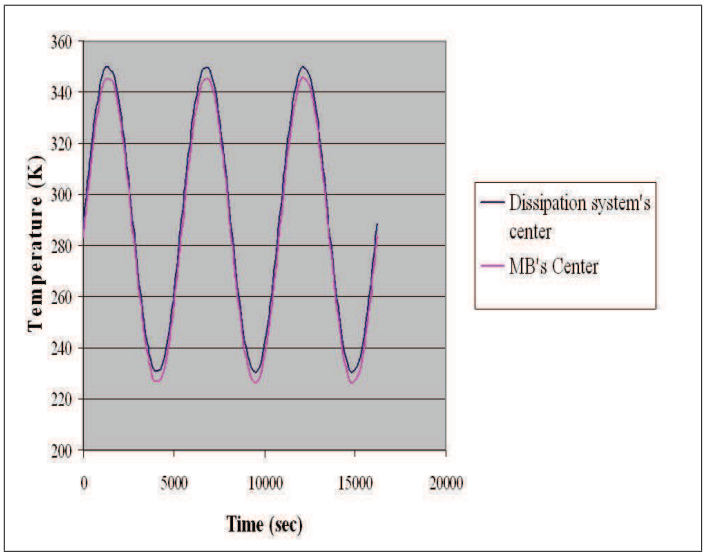

Figure 4.2: Temperature variation in the MB's center in compare with the DS's center during three cycles.

Table 4.1: Temperatures at different locations on the MB.

Location	Max. temperature (K)	Min. temperature (K)
MB's center	345.778	226.174
DS's center, MB's front	350.114	230.435
DS's center, MB's back	350.046	230.373

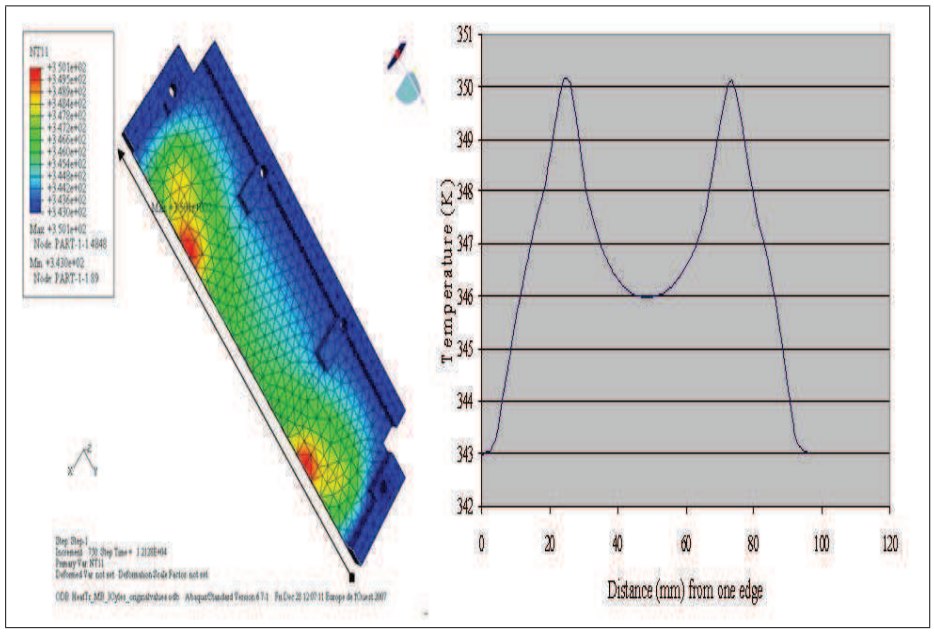

Figure 4.3: Temperature variation along a cross-section of the MB.

4.3 2-Dimensional creep analysis

Solder joints are often cause of failure in electronic devices, failure due to cyclic creep induced ductile fatigue. In the following, the results of 2-dimensional creep modeling of a cross-section of solder joints under thermal cycling condition, nominal and accelerated, in order to predict life time are presented.Temperature is applied using a *sin* function , Fig. 4.4, as a uniform field on the whole model.
Using the results of first analysis, temperature variation estimated by *sin* function, and the maximum temperature is 77 °C and minimum is equal to -47 °C, so a function which has a maximum of + 75 °C and a minimum equal to -55 °C is applied to the whole assembly, considering the point that a difference of a few degrees in temperature does not play so much role in creating stress and strain.
At this stage, an assumption has been made regarding temperature variation during accelerated test cycles; since there is no dissipation systems on the 0805 resistors' test vehicle, maximum and minimum temperature would be the same as outside temperature variation in the space: -50 °C to +70 °C, as it is also applied during the test, with a period equal to the duration of one cycle, 20 min, neglecting 10 seconds transfer time between two chambers.

First objective, is to identify the most critical areas in terms of induced stress and creep strain. Three regions in the solder joints are detected, end of solder under the component, beside the component's fillet, and solder's fillet, this is true for both real and test cycles, Fig. 4.5.

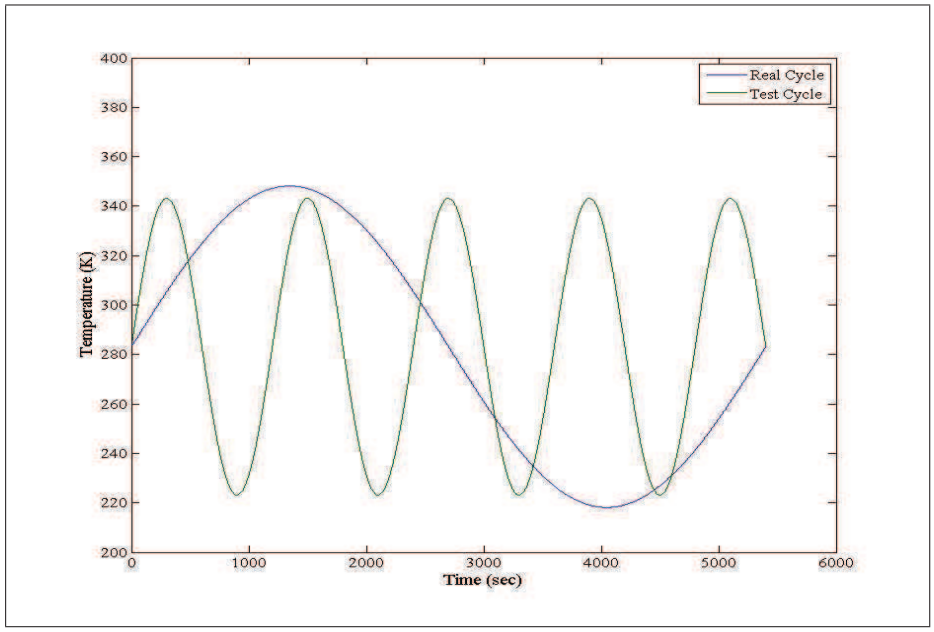

Figure 4.4: Temperature function for real and test cycle during one real cycle, one real cycle is equal to 4.5 test cycles in terms of duration, these functions are applied as the amplitude of temperature field in ABAQUS.

Two approaches could be followed for calculating life time, either taking the actual minimum (or average) over the path of local maximum equivalent creep strain [17], which is not exactly clear what it is!, or taking the node where induced accumulated creep strain reaches to the highest value during one cycle, which could be described as the worst case. Considering our special application, SwissCube's boards, where the reliability is a prime parameter, proceeding with second approach is reasonable, so the second node, see Fig. 4.5, is used to extract the accumulated creep strain.
A second step could be considered as determining the minimum number of cycles required for creep analysis. To answer this question an initial analysis has been performed for five real cycles using material properties of SnAgCu and SnPb, Fig. 4.6. As it is illustrated in the plot, after one cycle, there is a constant increase in accumulated creep strain, the same approach was followed for the test cycles, and it is also the case for test cycles. As a result, for further analysis three test cycles and two real cycles are simulated, and accumulated creep strain in the target node in order to predicting life time is extracted.

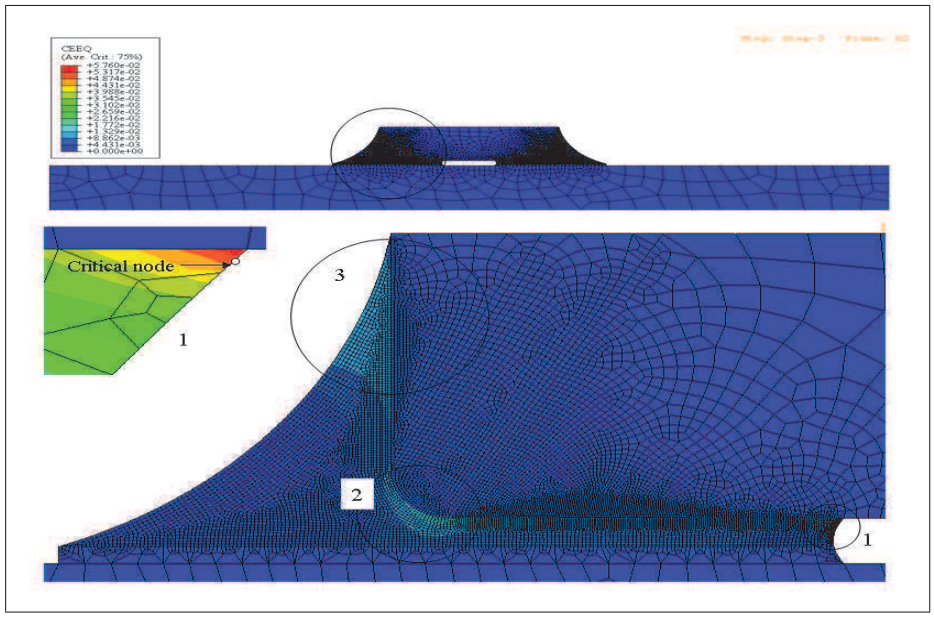

Figure 4.5: Three regions were identified as critical regions in terms of induced creep strain.

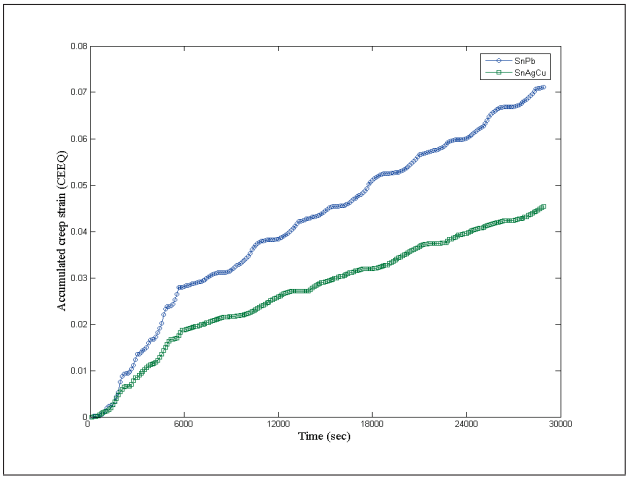

Figure 4.6: Accumulated creep strain for five real cycles, as it is clear first cycle is critical and creep accumulates faster.

A large number of simulations have been performed implementing solder's material properties and constitutive relations from different sources, see Sec. 2, from the results of each simulation accumulated creep strain for the aformentioned node has been extracted and using available life prediction relations the life time of solder joints have been predicted, Tables 4.3 and 4.2. Two frequently used life prediction relations for SAC are *Syed*'s relation and *Schubert*'s relation, and for SnPb *Schubert*'s, *Spraul*'s, and *Grivas*'s relations would be used.

Table 4.2: Life prediction results for SnAgCu solder joints in 2-dim., note that *Schubert*'s life prediction relation is different for SAC and SnPb

Cycle's type	Life prediction relation	SnAgCu [20]	[18]	[15]	[16]	[17]	[22]	[21]	*New*
Real	*Schubert*	1705	2049	954	1421	1798	3222	1746	1702
	Syed	1910	2201	1220	1659	1990	3122	1946	1907
Test	*Schubert*	2076	2777	1056	1824	2221	6080	2098	1955
	Syed	2224	2783	1320	1932	2342	5098	2242	2123

Table 4.3: Life prediction results for SnPb solder joints in 2-dim. note that *Schubert*'s life prediction relation is different for SAC and SnPb

Cycle's type	Life prediction prediction	SnPb [10]	[16]	[14]	[15]
Real	*Schubert*	3714	1280	1460	2112
	Spraul	2765	1410	1744	1936
	Grivas	4390	1373	1502	2374
Test	*Schubert*	5800	1378	1748	2327
	Spraul	3664	1479	1719	2058
	Grivas	7133	1491	1826	2638

As it was expected the new constitutive relation gives the lowest number of cycles to failure for SnAgCu, if a near approach is followed for SnPb, neglecting the highest and lowest band of the scatter, and taking *Pao*'s [14] constitutive relation as the reference, both solders tolerate more than one thousand cycles, since this result has been obtained by taking the safest assumptions, it is predicted that no failure would be observed after one thousand test cycles, and both solders would have even a much higher life time.
For SnAgCu, the stresses reach much higher values during the temperature cycling, resulting in higher hysteresis loops. Although the creep strain for SnAgCu during test is smaller (= width of the loop but the difference is very small in this case), the dissipated energy per cycle (= area in the loop) is higher due to the higher stresses. Fig. 4.7 shows the hysteresis loops for one normal and one shear stress/strain component and proves the upper statement.
For the *New* SnAgCu constitutive relation and *Pao*'s SnPb constitutive relation, the number of life cycles to failure, for other critical regions, Fig. 4.5 were calculated to see the risk of first calculation and the probability of crack propagation through the solder joints under the component or through the solder toward it's fillet edge. This was done for real cycles using *Scubert*'s prediction model which seems more critical. The results of this calculation are presented in Table 4.4. This proves how much first calculations were safe and conservative, and it is not expected to see any damage for one thousand test cycles, while the difference between two solders becomes bigger probably due to stress magnitude, since those areas have low stress values and in low stress regions SnAgCu gives lower creep strain, see Fig. 4.8.

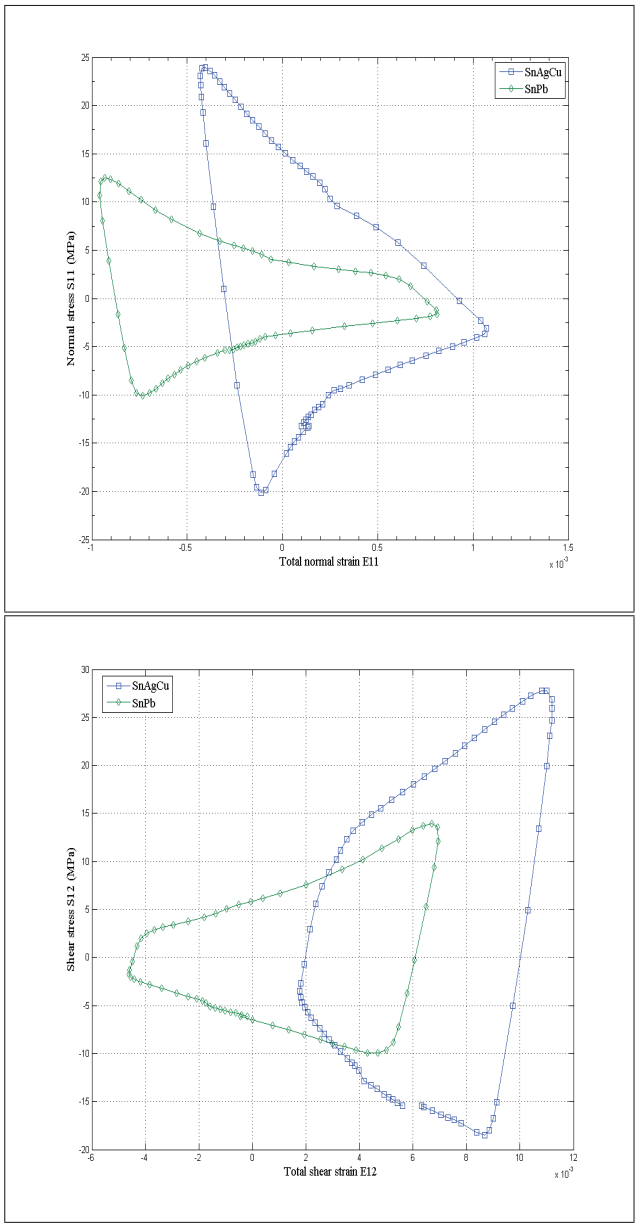

Figure 4.7: Stress-strain hysteresis loop for real cycles during 6^{th} cycle, for SnAgCu in compare to SnPb for one normal and one shear component of the stress and strain.

It was supposed to follow energy approach as well, and it was implemented for SnPb to calculate the number of life cycle to failure, Table 4.5. However, on one hand it is not clear if the ABAQUS' output, total creep energy density (ECDDEN) or other creep energy values, represent what should be used in energy laws, and on the other hand, the definition of these laws are not consistent in different resources.

Table 4.4: Number of cycles to failure for three critical regions of solder joints in 2-dimensional simulation using *Schubert*'s relation for life prediciton.

Node	1	2	3
SnAgCu	1702	11255	15770
SnPb	1460	6157	11691

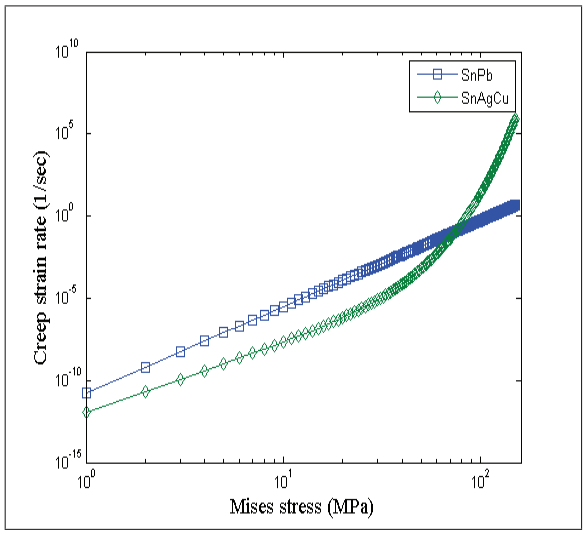

Figure 4.8: Creep strain rate for SnAgCu and SnPb, as it was mentioned there is a transition stress value, where below this value SnAgCu gives a lower creep strain rate, and above this value it gives a higher creep strain rate in compare to SnPb

Table 4.5: Number of life cycles to failure using energy approach.

Model	Constitutive relation							
	[10]	[16]	[14]	[15]	[10]	[16]	[14]	[15]
	Test cycles				Real cycles			
Schubert	1565	645	1616	920	1164	761	1842	1047
Spraul	3233	1495	3397	2054	2535	1734	3819	2306

4.4 3-Dimensional creep analysis

Using the results of 2-dimensional FE-analysis, *Pao*'s and *New* constitutive relations were implemented for SnPb and SnAgCu respectively in 3-dimensional analysis. In fact, 3-dimensional analysis is very time consuming and it is not possible to investigate the effect of refining mesh for this model, for example an analysis had been started using a very fine mesh, just for solder joints, but it did not progress more than 10% of one cycle during four days, it means a very powerfull computational resource is needed, otherwise, it will take even three or four weeks to complete one 3-dimensional simulation. The finnest applicable mesh was used and both tetrahedron and hexagonal, where ever it was possible due to geometery, were employed to get the results.

There is a small area around the end solder where it is in contact with package directly, on this area a large amount of shear strain is created, Fig. 4.9. Considering, the large CTE mismatch between epxy package (110 ppm/K) and FR4 (18.5 ppm/K), this big stress concentration seems reasonable.

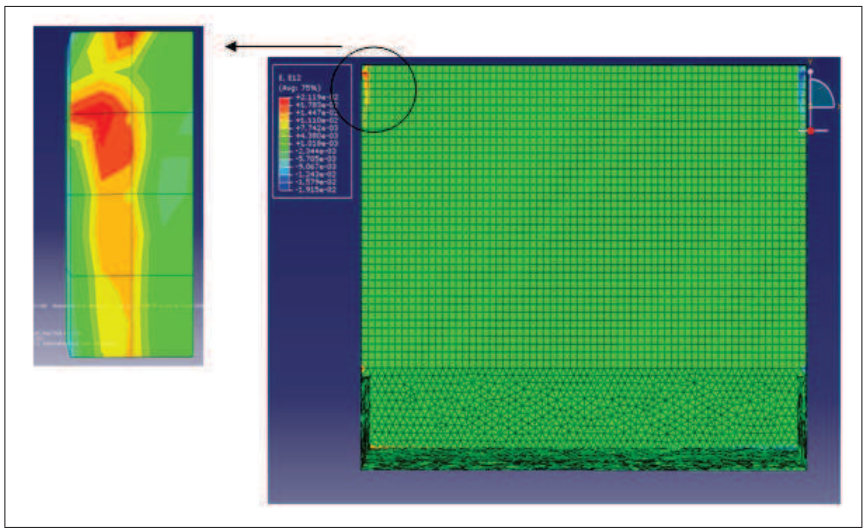

Figure 4.9: Shear strain in the solder joint under the package, 8 elements were picked to perform further analysis.

As a result, the life time would be very small for the solders, however, these are valid locally around the contact area with epoxy package. Seven regions were selected in the end solder or heat conductor, Fig. 4.10, and three regions, in the front solder or electrical connector, Fig. 4.11, were selected to extract accumulated creep strain and calculate number of life cycles to failure.
It is important to mention that if solder fails in one point where the number of cycles to failure is very low, for example in the first or third region of heat conductor or first region of electrical connector the component will not fail, because there is still enough solder under the package and failure of those points will not affect other points significantly. Especially, solder in a big area around region seven in heat conductor solder as well as region one in electrical connector will last for a very long time. As a result, the strain concentration area will not increase the risk of total failure. A comparison of the number of life cycles to failure for SnAgCu and SnPb, using *Schubert*'s equation, which gave lower values in 2-dimensional FE-analysis, are presented in Table 4.6 and 4.7.

Table 4.6: Number of life cycles to failure for different regions in heat conductor (end solder), one node in each region was selected.

Region	1	2	3	4	5	6	7
SnAgCu	95	1246	624	366	595	1623	11357
SnPb	19	1165	492	128	282	865	5220

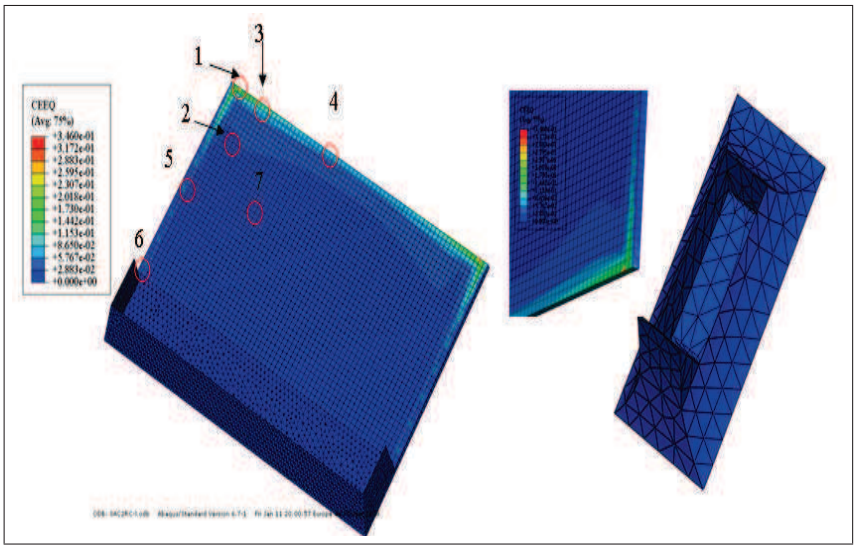

Figure 4.10: Different regions were selected to calculate the life time to failure in the heat conductor.

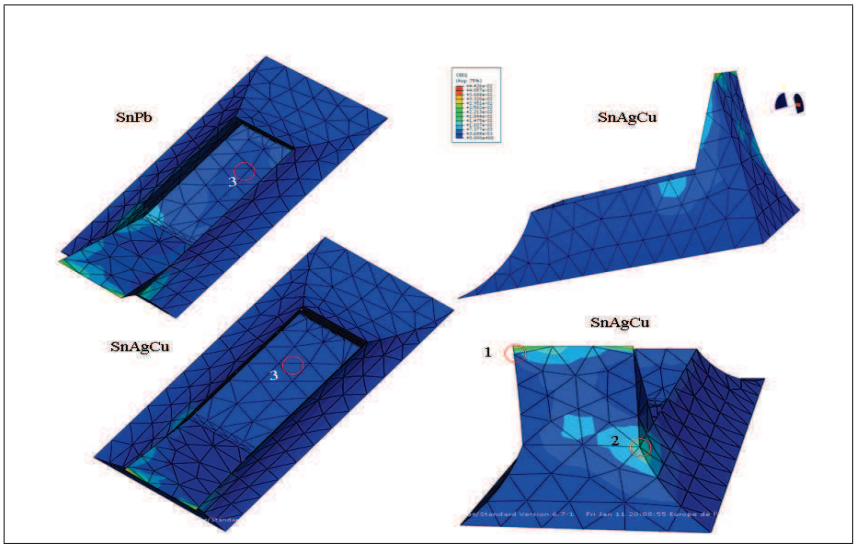

Figure 4.11: Different regions were selected to calculate the life time to failure in the electrical connector, as it is seen a larger amount of creep strain has been accumulated in SnPb.

Table 4.7: Number of life cycles to failure for different regions in electrical connector (front solder), one node in each region was selected.

Region	1	2	3
SnAgCu	1547	3392	98422
SnPb	865	2747	38702

Regarding, the induced stress in the solder joint, it was observed that, except around the epoxy package and region one in electrical connector (front solder) where there is a large stress concentration, the rest of the solder does not experience a large amount of stress Fig. 4.12. This stress concentration partly explains the results of creep modeling; locally, stress exceeds yeild criteria and not taking plasticity into account creates a large amount of creep strain which results in very low number of cycles to failure.

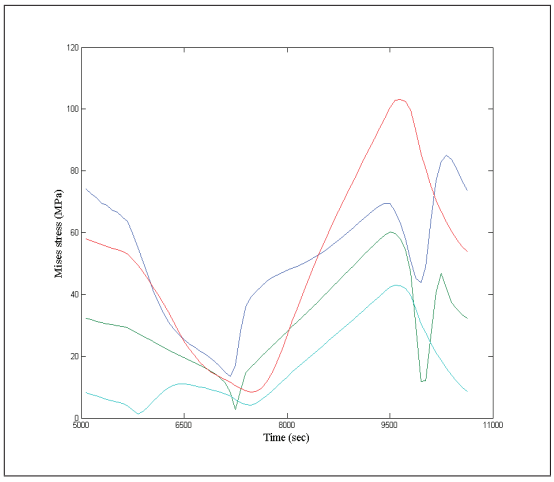

Figure 4.12: Mises stress evolution during second real cycle for different regions in the solder joints.

4.5 Experimental analysis

Due to time constraint thermal shock test was performed for one thousand cycles. Temperature was measured in the center of resistors board and on the dissipation system's board beside the resistor using thermocouples, a plot of temperature variation is illustrated in Fig. 4.13. Temperature on the resistor boards is like what was expected, -50°C to +70°C, while there is a small change dissipation systems' board's temperature, and that is because of difference in the number of dissipation systems and a completely different boundary condition in terms of heat transfer; in the space there is no heat transfer by convection, but during thermal shock test there is a forced convection heat transfer in both hot and cold chambers. Moreover, such a difference in the maximum temperature does not play so much role in the number of life cycles to failure, one simulation has been performed for SnAgCu to find out if there is a significant difference, Table 4.8.

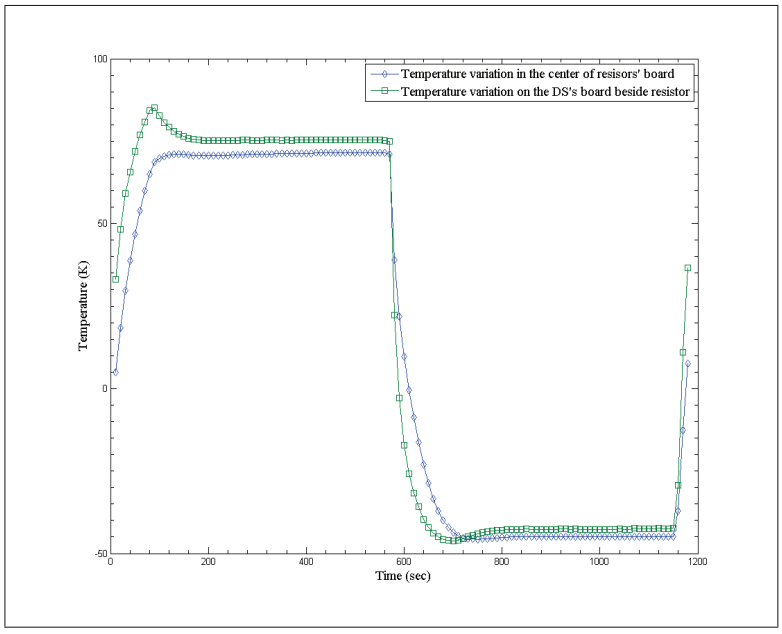

Figure 4.13: Temperature measurements results on the boards during last thermal cycle

Table 4.8: Number of life cycles to failure for SnAgCu using test results' temperature range.

Life prediction model	Test cycles range	
	-50 °C to +70 °C	-47 °C to +87 °C
Schubert	1955	1854
Syed	2123	2037

As it was expected no cut in voltages was observed, Fig. 4.14, note it does not show if there is a crack or not; it was proposed to monitor resistance change (on line or off line), but it was not possible due to the lack of enough facilities and resources.

4.5.1 Microstructural analysis

For microstructural analysis a metallography process proposed by EMPA[1] , see Appendix D, was followed firstly, to analyze solder joints, however the results were not as appropriate as what was expected before in terms of contrast. So, it was decided to take two groups of pictures, first group were taken after polishing and before etching, and second group were taken after etching process, then comparing the pictures resulted in keeping the pictures without etching.

[1] A materials science and technology research institution of the Swiss Federal Institute of Technology

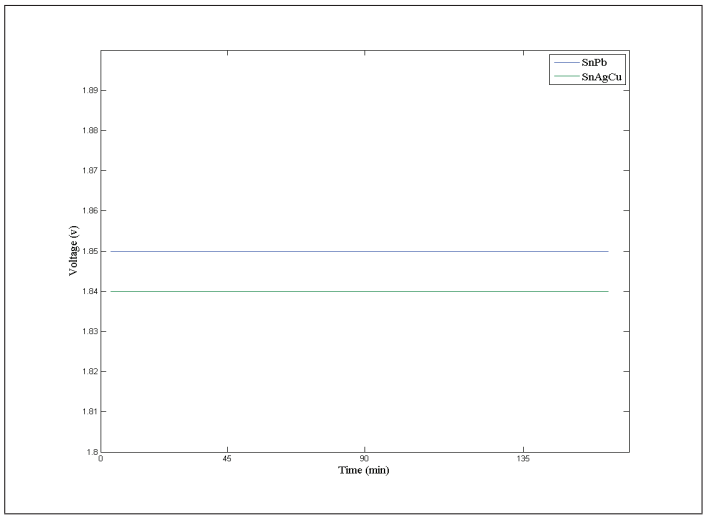

Figure 4.14: Voltage variation in the last 8 cycles for both solder joints, no change could be observed

As it is clear in the figures there is still good adhesion between surfaces and no major damage are evident in the bulk solder or under the packages. In addition to the number of cycles, it could be important to note that there is no solder or a few amount of it under the packages either big one or the small one, this is due to the type of soldering; on one hand it was not done precisely, and on the other hand it was not carried out from bottom to the top[1].

MP 725 power film resistor

There are some holes under film resistors, in the case of SnPb, no damage was observed in the front solder (electrical connector) either in front of the gull wing leads or under gull wing leads, and the microstructure seems fine Fig. 4.15, moreover interphase layer between solder and gull wing leads seems clear, and thin.

In the end solder (heat conductor), Fig. 4.16, generally microstructure seems uniform, no crack or damge was identified, this agrees with the simulation which suggests problem comes from under packge. Under the package, some intermetalics were formed in the interfacial layer, either between solder and package or between solder and copper. It should be noted that it could be a composition with gold, since the surface finish is Ni/Au. The composition should be determined using other methods such as energy dispersive X-ray spectroscopy (EDX). There is also a crack which is assumed originally comes from manufacturing process. Probably, two big holes were created first, and then joining these two holes created a big crack. It must be noted that polishing has been done three times, and this crack is still present.

[1]Reflow soldering is the most common means to attach a surface mounted component to a circuit board, and typically consists of applying solder paste, positioning the devices, and reflowing the solder in a conveyorized oven [2].

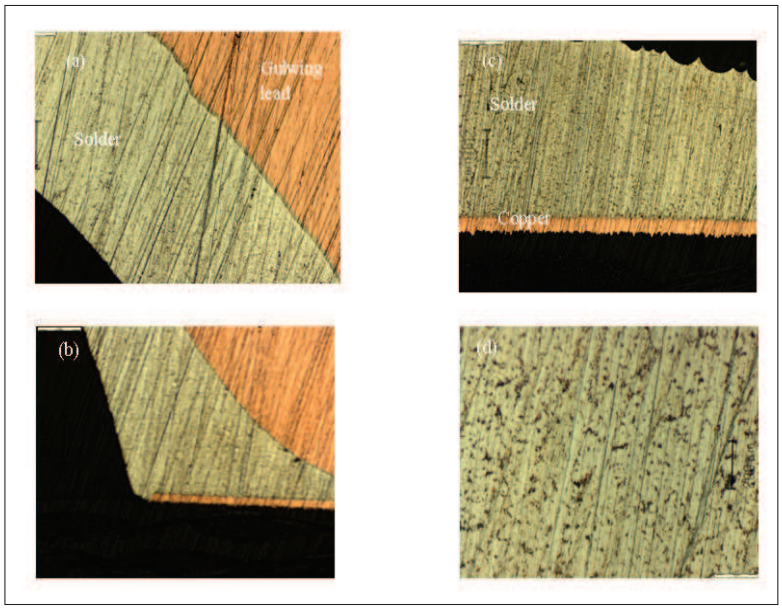

Figure 4.15: Solder's (SnPb) microstrauture using optical microscopy, (a) Upper half of solder under gull wing lead, (b) Lower half of solder under gull wing lead, (c) Solder in front of the gull wing lead, (d) Microstructure of the SnPb solder under gull wing lead.

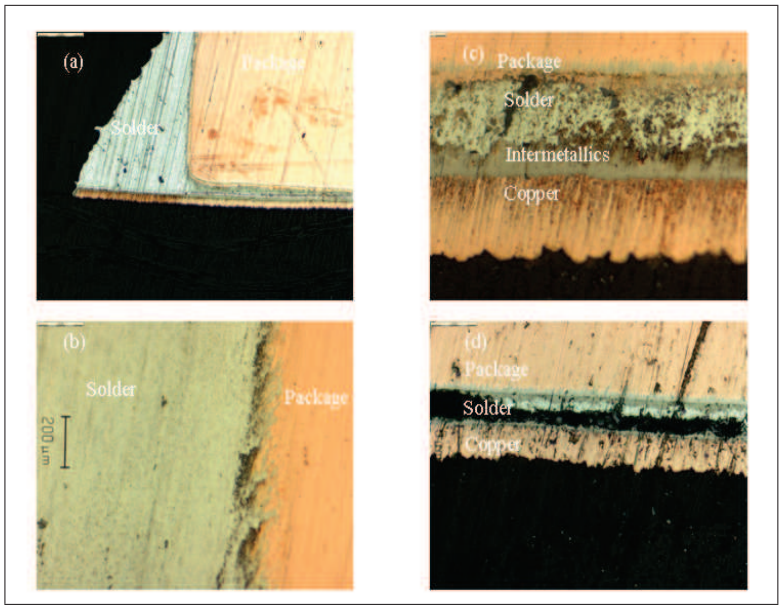

Figure 4.16: Solder's (SnPb) microstrauture, (a) At the end of the package, (b) No crack is observed in the interfacial layer,(c) An intermetalic layer has been formed between solder and copper, (d) A big crack has been formed through the solder under package.

For SnAgCu the situation is the same for front solder joints, Fig. 4.17, the microstructure is uniform and no damage is observed. Under gull wing leads, is where some damage has been reported by other researchers, for example [3]. In the end solder, the microstructure does not show a significant deformation, but under the package there are some holes mainly due to manufacturing process, and a sharp crack is observed through the interfacial layer between solder and package, where maximum shear strain is created. It must be note that either for SAC or tin-lead there are alot of microvoids under the packages.

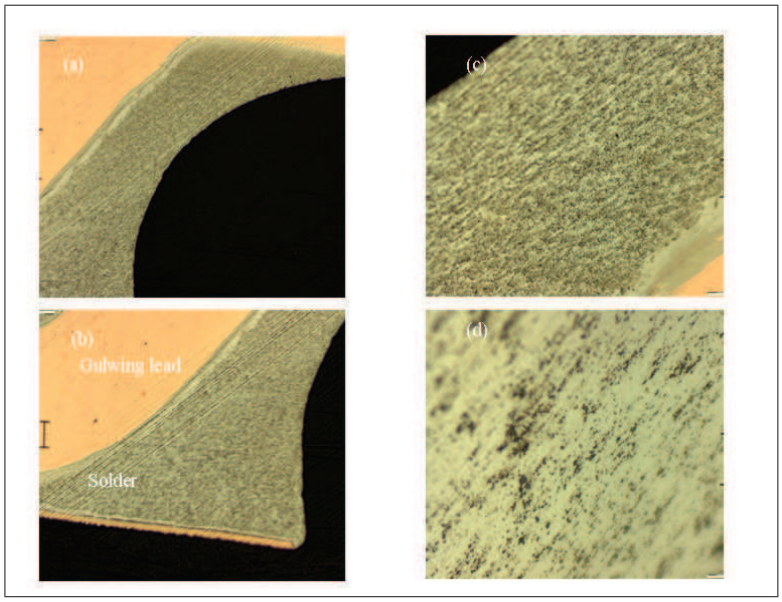

Figure 4.17: Solder's (SAC) microstrauture,(a) Upper half of solder under gull wing lead, (b) Lower half of solder under gull wing lead,(c) Solder under gull wing lead , (d) Microstructure of the SnAgCu solder under gull wing lead using optical microscopy.

0805 resistor

For small resistors, again there is no damage around the package, Fig. 4.19 for SnPb, moreover microstructure seems fine and no damge or crack is observed. Generally speaking, there is a few amount of solder under these small packages, which is not standard; there are a few cases where enough solder was observed under the resistor. There is an intermetalic layer between solder and copper (and Ni/Au), however, in one case it was observed that it is not continuous through the solder joint for SnPb, and a crack (or hole) was created under the package, however it is supposed that it started from manufacturing defects.

Around the package, and beside fillet, solder's microstructure shows no damage, however, under the package solder layer is very thin, generally less than what is observed here. In a few cases where there are enough solder, no major damage is observed. Microvoids have been formed in the solder especially under the package. There is a layer between solder and copper, probably Ni/Au, but in contrast with MP725, phases are separated clearly.

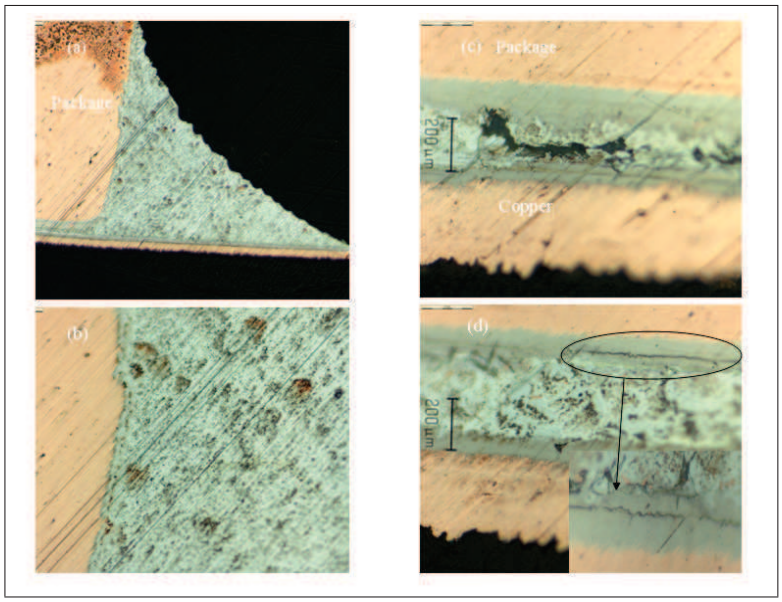

Figure 4.18: Solder's (SAC) microstrauture, (a) At the end of the package, (b) No crack is observed in the interfacial layer, (c) A big crack; probably it has been formed joining two holes, (d) A sharp crack has been formed in the interfacial layer between package and solder.

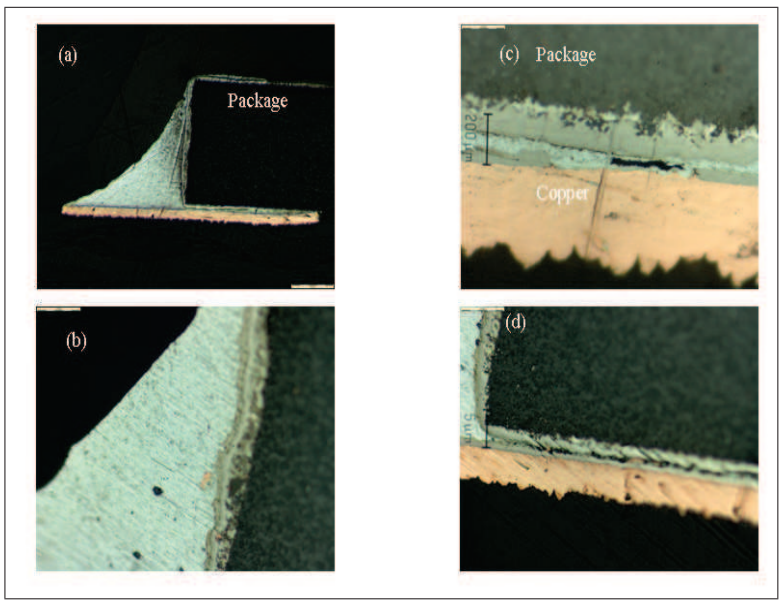

Figure 4.19: Solder's (SnPb) microstrauture, (a) One solder joint, (b) A micro-section from the fillet, (c) A big hole probably due to the lack of enough solder, moreover the intermetalic is not continuous, (d) Thickness of the solder under the package.

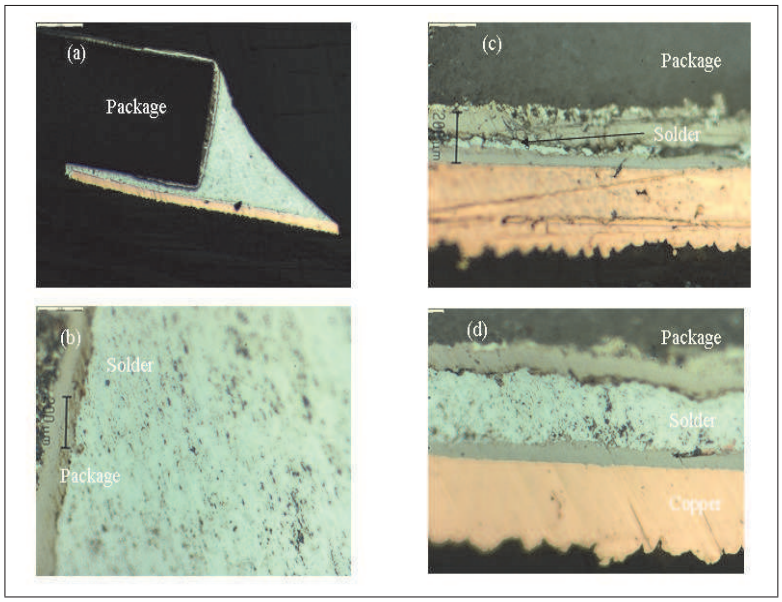

Figure 4.20: Solder's (SAC) microstrauture, (a) One solder joint, (b) A microsection from the fillet, (c) Thickness of the solder under the package, (d) Microstructure does not show significant deformation.

4.6 Discussions

For thermal modeling some assumptions were made like boundary conditions, and according to these assumptions which were approved by SwissCube's engineers temperature was simulated with a *sin* function. The results show that temperature changes with the same function, and maximum will not exceed a certain acceptable range (-50 °C to +90 °C). Thermal modeling analysis showed the effect of having copper in FR4 is more important than other parameters; actually, copper facilitates heat transfer hugely (around 150%).
In 2-dimensional creep modeling, the effect of having different constitutive relations seems more critical than using different life prediction models Fig. 4.21, this could justify the importance of choosing an appropriate constitutive equation, and clarifies the importance of experimental characterization of solder alloys.
The second point is about failure of solder joints (in 2-dimension), three regions were determined having the maximum amount of creep accumulation, with a significant difference. This results in having a low risk of failure after seeing the first failure Fig. 4.22, under the package close to joint's corner, due to the type of loading which is thermal[1]. In 3-dimensional analysis, a large amount of creep strains were developed in different regions under the package or in one region of electrical connector (front solder). However, if we consider the number of life cycles versus the risk of total failure Fig. 4.23, where the risk of total failure is very high, in the center of the end solder (heat conductor) or under gull wing lead (region one), the number of life cycles for both solders' compositions is very high, that makes them safe to be used in this application.

[1]Thermal loads means joints are loaded because of CTE mismatch (strain based loads), and failure at one point does not change load's magnitude at other points significantly.

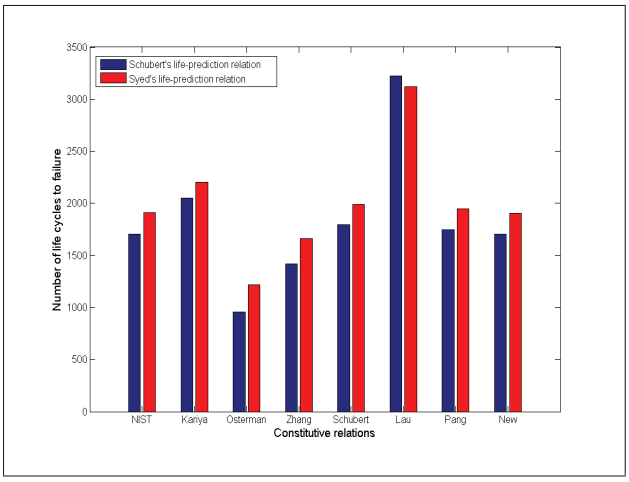

Figure 4.21: Effect of different constitutive relations in compare with different life prediction models.

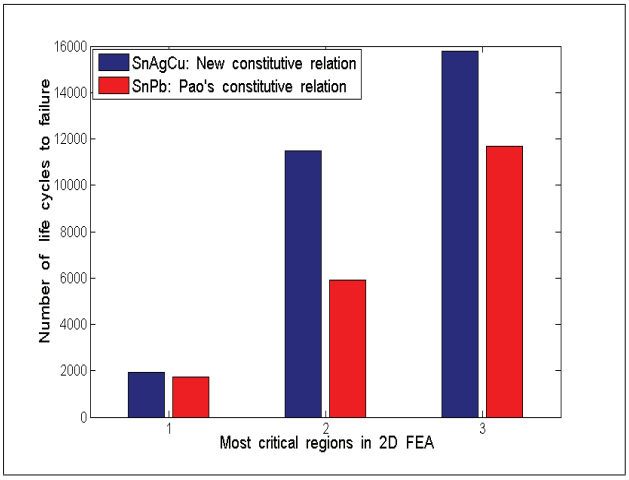

Figure 4.22: Number of life cycles to failure for 3 different regions where maximum creep strain is induced.

Considering the micrographs, generally SnAgCu shows finer microstructures, but it would not be clear as long as further analysis, for example SEM using EDX, was not done. Generally speaking, both solders would tolerate one thousand cycles with no clear damage.
For practical reasons, thermal shock test was performed only for one thousand cycles while it is necessary to do a test which lasts for at least five thousand cycles, to see the effects of having creep deformation or other deformation mechanisms clearly. It was not possible to investigate microstructure before thermal test due to the same reasons, while it is recommended to microstructral analysis before and after test to have a better idea of changes in the microstructure.It is suggested to monitor resistance change, on-line or off-line, to have a good idea about the crack propagation inside the solder joints.

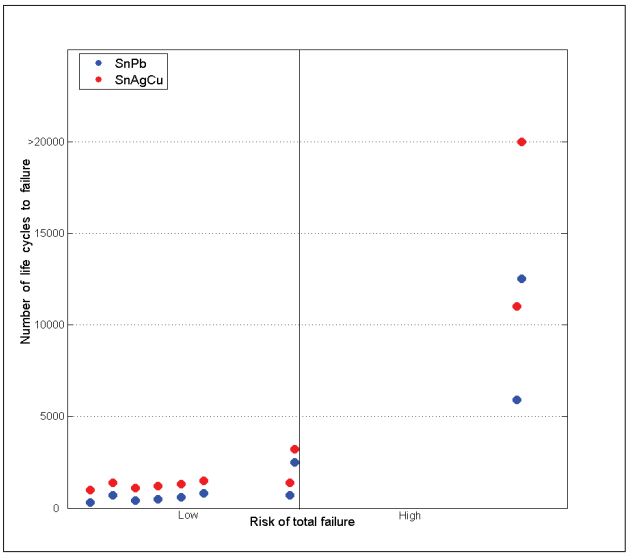

Figure 4.23: Number of life cycles are shown for different regions according to their contribution to the total failure, as it is clear where the risk of failure is high the number of life cycles to failure is really high.

Chapter 5

Conclusions

5.1 Conclusions

This thesis' main objective was to examine lead-free solder joints' (SnAgCu) reliability under thermal loadings, in order to evaluate the possibility of replacing old tin-lead composition with the new one, targeting an aerospace application, where there is still no directives to limit using toxic materials. Reviewing literature, specifically under thermal loads lead-free solders are generally more reliable than tin-lead compositions. This varies from application to application which makes it necessary to examine each case individually.
As a part of this thesis, temperature variation of the SwissCube's mother board (MB) was simulated. Some assumptions were made and temperature was determined for different locations on the board. Results, suggest that temperature will not exceed an acceptable extreme (-50 °C +90 °C) regarding functionality of electrical devices.
In the second part of this work, deformation of solder joints under thermal loads were simulated. It is well documented in the literature that creep plays the most important role where solder joints are thermally loaded. To simulate creep deformation of lead-free solders a new constitutive relation was fitted to all adequate available constitutive relations to have the worst case in terms of creep accumulation. Taking into account temperature variation from first analysis, creep deformation was determined using a finite-element software (ABAQUS 6.5 and 6.7), in 2-dimension for a small package, 0805 resistor. Results show that both SnPb and SnAgCu would withstand this type of loading for a long number of life cycles, and safe enough to be used up to 2000 cycles at least. All major constitutive relations were implemented to the finite-element analysis. It was shown in 2-dimensional analysis, that solder does not experience so much stress. This could justify why SnAgCu shows a higher life time.
In the third part of this thesis, an important package was considered for creep analysis. Two constitutive relations were selected from 2-dimensional analysis and creep deformation was calculated using ABAQUS 6.7, considering the worst possible situation in materials' properties' and geometry terms. Actually, simulation shows the solder joints will last significantly more than 10000 cycles (more than 20 months) in the case SnAgCu and more than 5000 cycles (more than 10 months) for SnPb, either for electrical connectors or heat conductors,

which satisfies first SwissCube's mission requirement (3 months). In the case of electrical connectors, the results of simulation shows that using SnAgCu is safe for a very long time.
In the last part of this work, an experiment was designed and performed to assess the reliability of solder joints under thermal shock test. For this special application a certain type of temperature cycles which guarantees reaching to the maximum and minimum temperature in the space was used. Temperatures were monitored on the test boards which show a good agreement with thermal simulations. Voltages were also monitored, and no cut was observed, it means no major failure was observed as it was expected from finite-element analysis. Under different packages, some holes and cracks were observed; this agree with the result of simulation which suggest that under package is the most critical area in terms of induced creep strain.
Overall speaking, using either SnAgCu or SnPb is safe for one thousand thermal cycles, and surely no cut in the circuits will be observed for less than this number of cycles. This is true for the worst case considered in this study, and it is predicted that solder joints would last at least for 4000 cycles (more than 8 months) which completely fulfills SwissCube's mission requirements. It is recommended to use SnAgCu, since solders are thermally loaded rather than mechanically and stress level is generally low, except in a few locations under the package close to the edge where the risk of failure is not high.

5.2 Future works

The main contributions that could be done to this project are listed below:

- New boundary conditions could be examined for thermal modeling; for example it is suggested to model temperature variation with *Modulated*[1], or other types of functions which present the temperature variation more precisely.
- The situation of test condition could be simulated, using heat transfer by convection.
- In-2-dimensional analysis of solders other geometries as well as other life prediction methods such as energy partitioning methods could be implemented.
- In the current models, 2-dimensional or 3-dimensional, the effects of changing material properties on induced creep strain and life cycles could be investigated.
- Other types of loadings could be simulated, to see the creep propagation and life time under a combined thermal and mechanical load.
- In 3-dimensional model the effect of changing current geometry could be investigated.
- An interesting contribution to the 3-dimensional modeling could be made by adding plasticity to the current model.

[1]It could be defined in ABAQUS using two *sin* functions.

- Parameters of this thermal shock test, such as cycle duration or dwell time at maximum temperature, could be changed to study th effect of these parameters on the solder joints.
- It is recommended to perform a vibration test for SwissCube's boards to examine the reliability of both solder compositions under mechanical loads, or both thermal and mechanical tests could be done in series.
- The effect of using reflow soldering[1] on the reliability of solder joints could be investigated as well.

[1] Reflow soldering is the most common means to attach a surface mounted component to a circuit board, and typically consists of applying solder paste, positioning the devices, and reflowing the solder in a conveyorized oven [2].

Appendix A

PCB Layouts

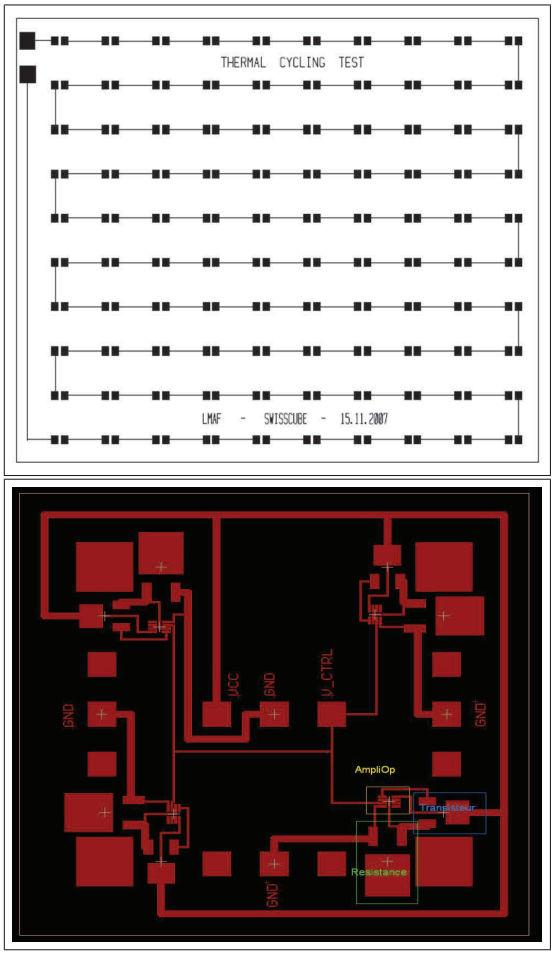

Figure A.1: PCB layouts for thermal shock test, dissipation systems' layout has been designed by D. Legancher.

Appendix B

Thermal shock test's preparation

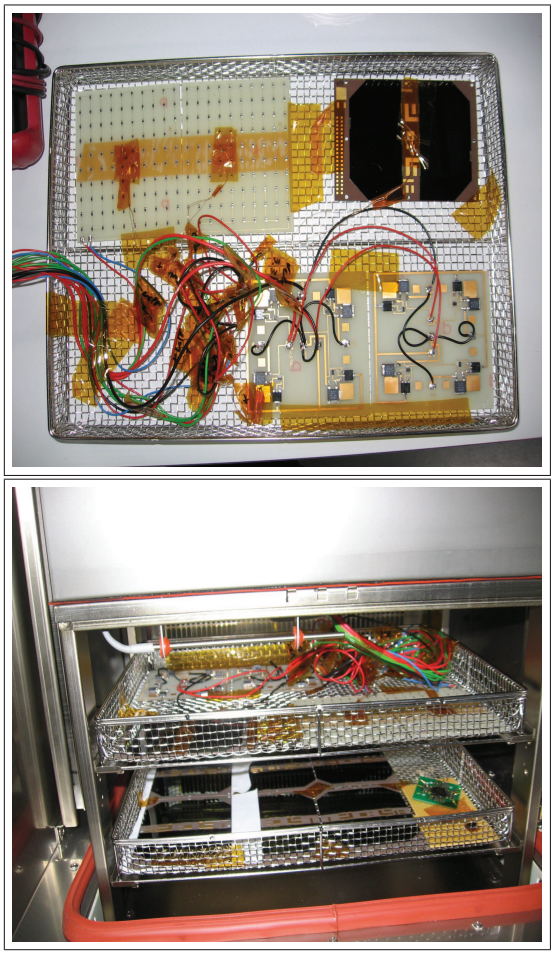

Figure B.1: Boards are put on a basket, then baskets are put in the oven, baskets are moving from hot to cold chambers and vice-versa automatically, thermocouples are plced in the middle of the boards and beside reistor, pictures have been taken by by D. Legancher.

Appendix C

Evaluating effects of different parameters on temperature variation in the SwissCube's motherboard

Thermal conductivity (eW/mmK)	Specific heat (eJ/tK)	Density (Tonnes/mm^3)	Thickness (mm)	Surface heat flux (eW/mm^2)	CTE (ppm/K)	Max. Tem. (K)	Min. Tem. (K)
49.79	8.79E8	2.87E-9	0.8	21.6	14.3125	350.114	230.373
					7	346.947	223.137
					28	350.12	223.146
			1.6		14.3125	344.691	223.09
		5.74E-9	0.8			350.065	223.136
		4..5E8				346.934	123.792
	13E8					350.069	223.141
100						346.596	223.125
25						356.953	223.1
14.3125				32.4		353.742	227.551
0.62	9.5E8	2E-9	0.8	21.6	14	874.517	231.165

Where there is no value, it means last value of that property is valid.

Appendix D

Metallography process

- Step1: Joint samples were carefully cut using the cutting machine to fit the sample holders.
- Step2: Clean the samples with ethanol, dry them and place them in the sample holders.
- Step3: Cold Mounting- Mix the required amount of Epoxy and Resin (Standard ratio). Pour them in the sample holder and leave them overnight.
- Step4: Grinding and Polishing- Samples were initially grinded in five stages with SiC papers and 300rpm machines. (80, 220, 600, 1000, 2400). Final polishing with cloth polishing machines with 3 and 1 micron suspensions with diamond paste. To get a finer view even at higher magnification sample was polished with 0.1 micron alumina suspension.
- Step5: Finally samples required an etching with 0.5
- Step6: Wash clean with running water followed by ethanol and dry the sample for observation

Bibliography

[1] Stam, F. A., Davitt, E., *Effects of thermo and thermomechanical loadings on the tin-lead and lead-free (SnPb and SnAgCu) surface mount joints*, Microelectronics Reliability 41 (2001) 1815-1822.

[2] Wikipedia, the free encyclopedia, http://en.wikipedia.org/wiki/Reflow_soldering.

[3] Xia, Y., Xie, X., *Reliability of lead-free solder joints with different PCB surface finishes under thermal cycling*, Journal of Alloys and Compounds, doi:10.1016/j.jallcom.2006.12.098, 2007.

[4] Engelmaier, W., *Reliability of lead-free (LF) solder joints revisited*, Global SMT and Packaging, v 3, n 8, November, 2003, p 34-35.

[5] Nurmi, S.,Sundelin, J., Ristolainen, E., Lepisto, T., *The effect of solder paste composition on the reliability of SnAgCu joints*, Microelectronics Reliability 44 (2004) 485494.

[6] Song, H. G., Morris Jr.,J.W., and Hua, F., *Creep properties of Pb-free solders*, Lawrence Berkeley National Laboratory, University of California, Berkeley, 2002.

[7] Wikipedia, the free encyclopedia: http://en.wikipedia.org/wiki/Creep_%28deformation%29.

[8] National Institute of Standards and Technology: http://www.metallurgy.nist.gov/solder.

[9] Syed, A., *Predicting Solder Joint Reliability for Thermal, Power, & Bend Cycle within 25% Accuracy*, Electronic Components and Technology Conference 2001.

[10] R. Darveaux and K. Banerji, *Constitutive relations for tin-based solder joints*, IEEE Transactions on Components, Hybrids, and Mnufacturing Technology, Vol. 15, No. 6, 1992.

[11] Darveaux, R., Banerji, K., Mawer, A. and Dody, G., *Reliability of plastic ball grid array assemblies*, Chap. 13, Ball Grid Array Technology, ed. J. H. Lau, McGraw-Hill, 1995, pp. 379-442.

[12] Frost and Ashby, *Deformation mechanism maps*, New York, Pergamon, 1982, Ch. 2.

[13] Meyers, M. A., and Chawla, K. K., *Mechanical metallurgy, principles and applications*, Englewood Cliffs, NJ: Prentice Hall, 1984.

[14] Pao, Y.H. (Ford Motor Company); Badgley, S.; Govila, R.; Jih, E., *Experimental and modeling study of thermal cyclic behavior of Sn-Cu and Sn-Pb solder joints*, Materials Research Society Symposium Proceedings, v 323, Electronic Packaging Materials Science VII, 1994, p 153-158.

[15] Osterman, M., Dasgupta, A., *Life expectancies of Pb-free SAC solder interconnects in electronic hardware*, J Mater Sci: Mater Electron (2007) 18:229236.

[16] Zhang, Q., Dasgupta, A., Haswell, P., *Viscoplastic Constitutive Properties and Energy-Partitioning Model of Lead-Free Sn3.9Ag0.6Cu Solder Alloy*, Electronic Components and Technology Conference, IEEE, 2003.

[17] Schubert, A., Dudek, R., Auerswald, E., Gollhardt, A., Michel, B., Reicbl, H., *Fatigue Life Models for SnAgCu and SnPb Solder Joints Evaluated by Experiments and Simulation*, Electronic Components and Technology Conference, IEEE, 2003.

[18] Kariya, Y. and Plumbridge, W. J., "Mechanical properties of Sn-3.0mass%Ag-0.5mass%Cu alloy", Proceedings, 7th Symposium on Microjoining and Assembly Technology in Electronics, Feb. 1-2, Yokohama, Japan, pp. 383-388, 2001.

[19] Neu, R. W., Scott, D. T. and Woodmansee, M. W., "Thermomechanical behavior of 96Sn-4Ag and Castin Alloy", ASME Transactions, Journal of Electronic Packaging, Vol. 123, No.3, September 2001, pp. 238-246.

[20] http://www.nist.gov/.

[21] Pang, J. H. L. and Xiong, B. S., *Mechanical Properties for 95.5Sn3.8Ag0.7Cu Lead-Free Solder Alloy*,IEEE Transactions on components and packaging technologies, 2005.

[22] Lau, J., W. Dauksher, and P. Vianco, *Acceleration models, constitutive equations, and reliability of lead-free solders and joints*, in Proc. IEEE ECTC Conf. 2003, pp. 229236.

[23] Wiese, S., et al., *Microstructural Dependence of Constitutive Properties of Eutectic SnAg and SnAgCu Solders*, 53^{rd} ECTC 2003, pp. 197-206.

[24] Syed, A., *Accumulated Creep Strain and Energy Density Based Thermal Fatigue Life Prediction Models for SnAgCu Soler joints*, published in ECTC 2004 conference proceedings (pp 737 - 746).

[25] Syed, A. R.,*ACES of Finite Element and Life Prediction Models for Solder Joint Reliability*, Design and Reliability of SolderS and Solder Interconnections, Proceedings of Symposium 1997 TMS Conference, pp. 347-355.

[26] http://www.plextek.co.uk/ltcc.htm.

[27] Spraul, M., Nuchter, W., Moller, A., Wunderle, B., Michel, B., *Reliability of SnPb and Pb-free flipchips under different test conditions*, Microelectronics Reliability 47 (2007) 252258.

[28] Vandevelde, B., Gonzalez, M., Limaye, P., Ratchev, P., and Beyne, E., *Thermal cycling reliability of SnAgCu and SnPb solder joints: a comparison for several IC-packages*, Microelectronics Reliability 47 (2007) 259265.

[29] Vandevelde, B.,Beyne, E., Zhang,G. Q., Caers, J. , *Solder parameter Sensitivity for CSP Life-Time Prediction using Simulation-Based Optimisation method*, Proceedings of the 51st Electronic Components and Technology Conference, pp. 281-287, 29 May - 1 June 2001, Lake Buena Vista, Florida, USA.

[30] Sundelin, J. J., Nurmi, S. T., Lepisto, T. K., and Ristolainen, E. O., *Effect of PCB surface finish on creep properties of lead-free solder joints* Soldering & Surface Mount Technology 17/4 (2005) 39.

[31] Nishiura, M., Nakayama, A., Sakatani, S., Kohara, Y., Uenishi, K. and Kobayashi, K.F., *Mechanical strength and microstructure of BGA joints using lead-free solders*, Materials Transactions, Vol. 43 No. 8, pp. 1802-7, 2002.

[32] Li, L., Jang, J-W. and Allmen, B., *Shear property and microstructure evaluation of Pb-free solder bumps under room temperature and multiple reflow/high temperature aging*, Proceedings of the 7th IEEE International Symposium on Advanced Packaging Materials, 2001, pp. 347-53, Braselton, GA.

[33] Ratchev, P., Vandevelde, B., and De Wolf, I., *Reliability and Failure Analysis of SnAgCu Solder Interconnections on NiAu Surface Finish*, Proceedings of 10^{th} IPFA 2003, Singapore.

[34] Xie, D., Geiger D., Arra, M., Shangguan, D., and Phan, H., *Reliability of CSP/Lead free solder joints with different surface finishes and reflow profiles*, SEMI Technology Symposium: Iternational Electroncs Manufacturing Technology (IEMT) Symposium, SEMICON West 2002.

[35] Wong, B., Helling, D. E., and Clark, R. W., *A Creep- Rupture Model for Two-Phase Eutectic Solders*, IEEE CHMT-11,No.3, pp. 284-290, 1988.

[36] Syed, A.*Reliability and Au Embrittlement of Lead Free Solders for BGA Applications*, Proc. Intern. Symposium and Exhibition on Advanced Packaging Materials, Braselton, Georgia, USA, March 11-14, 2001, pp. 143-147.

[37] Mawer, A. J., Nick Vo, Johnson, Z., Lindsay, W., *Board-Level Characterization of 1.0 and 1.27 mm Pitch PBGA for Automotive Under-Hood Applications*, Proceedings 49th Electronic Components and Technology Conference, 1999.

[38] Mechanical ICD prepared by Roethlisberger, G., SwissCube documentations, Space Center, EPFL, Lausanne, Switzerland, 2007.

[39] Wikipedia, the free encyclopedia, http://en.wikipedia.org/wiki/Radiation.

[40] Ridout, S., and Bailey C. *Review of methods to predict solder joint reliability under thermo-mechanical cycling*, Fatigue Fract Engng Mater Struct 30, 400412, 2006.

[41] IPC-SM-782, Surface Mount Design and Land Pattern Standards, Section 8, 93.

[42] http://www.matweb.com/.

[43] http://www.caddock.com/.

[44] Space product assurance, High-reliability soldering for surface-mount and mixed technology, ECSS-Q-70-38A, 26 October 2007.

[45] Wikipedia, the free encyclopedia, en.wikipedia.org/wiki/Surface-mount_technology.

[46] Prof. Carol, *Mechanics and materials*, http://ocw.mit.edu/NR/rdonlyres/B232C6DD-0629-4804-9814-1AF87560D706/0/lec14.pdf.